Petroleum Science 19 (2022) 2741–2756

Contents lists available at ScienceDirect

Petroleum Science

journal homepage: www.keaipublishing.com/en/journals/petroleum-science

Original Paper

Low-field NMR inversion based on low-rank and sparsity restraint of relaxation spectra

Si-Hui Luo [a, b], Li-Zhi Xiao [a, b, *], Yan Jin [a, b], Jiang-Feng Guo [b], Xiao-Bo Qu [c], Zhang-Ren Tu [c], Gang Luo [a, b], Can Liang [d]

[a] College of Artificial Intelligence and College of Petroleum Engineering, China University of Petroleum, Beijing, 102249, China
[b] State Key Laboratory of Petroleum Resources and Prospecting, China University of Petroleum, Beijing, 102249, China
[c] School of Electronic Science and Engineering (National Model Microelectronics College), Xiamen University, Fujian, 361005, China
[d] Changzhou Institute of Technology, Changzhou, Jiangsu, 213000, China

A R T I C L E I N F O

Article history:
Received 20 June 2022
Received in revised form
18 September 2022
Accepted 25 October 2022
Available online 4 November 2022

Edited by Jie Hao

Keywords:
Low-field NMR
Inversion method
Low-rank and sparsity restraint
Relaxation spectra
Data processing

A B S T R A C T

In this paper, we proposed a novel method for low-field nuclear magnetic resonance (NMR) inversion based on low-rank and sparsity restraint (LRSR) of relaxation spectra, with which high quality construction is made possible for one- and two-dimensional low-field and low signal to noise ratio NMR data. In this method, the low-rank and sparsity restraints are introduced into the objective function instead of the smoothing term. The low-rank features in relaxation spectra are extracted to ensure the local characteristics and morphology of spectra. The sparsity and residual term are contributed to the resolution and precision of spectra, with the elimination of the redundant relaxation components. Optimization process of the objective function is designed with alternating direction method of multiples, in which the objective function is decomposed into three subproblems to be independently solved. The optimum solution can be obtained by alternating iteration and updating process. At first, numerical simulations are conducted on synthetic echo data with different signal-to-noise ratios, to optimize the desirable regularization parameters and verify the feasibility and effectiveness of proposed method. Then, NMR experiments on solutions and artificial sandstone samples are conducted and analyzed, which validates the robustness and reliability of the proposed method. The results from simulations and experiments have demonstrated that the suggested method has unique advantages for improving the resolution of relaxation spectra and enhancing the ability of fluid quantitative identification.

1. Introduction

Nuclear magnetic resonance (NMR) is a well-known and sophisticated technology, and has been widely applied to many scientific fields, such as chemical engineering, material science, medicine, agriculture, space science and etc (Casanova et al., 2011; Johns et al., 2013). Nowadays, NMR has been an indispensable technique and a gold tool for the reservoir exploration and development in petroleum industry (Song and Kausik, 2019). With the capability to directly detect the dynamics of fluid molecules in porous rocks, petrophysical parameters, such as pore structure, permeability (Jin et al., 2020), fluid mobility (Pang et al., 2017), fluid property (Singer et al., 2017), wettability (Liang et al., 2019) and etc., can be effectively obtained. Those parameters are of great significance to the key issues like oil/gas detection, drilling/completion scheme, reservoir evaluation and oil recovery during the process of oil/gas exploration and development. For instances, wireline NMR (Coates et al., 1999) and logging while drilling NMR (Hursa et al., 2020) for real-time reservoir evaluation, NMR rock core analysis for the study of hydration process and mechanism of oil well cements (Liu et al., 2021), and the monitoring process of fluid/gas flooding by using NMR system for quantifying the oil recovery rate (Siavashi et al., 2022), are all hot topics in petroleum industry nowadays.

In practical applications, Carr-Purcell-Meiboom-Gill (CPMG) pulse sequence (Carr and Purcell, 1954; Meiboom and Gill, 1958) and its variants are normally used as the basic detection means to

* Corresponding author. College of Artificial Intelligence and College of Petroleum Engineering, China University of Petroleum, Beijing, 102249, China.
E-mail address: xiaolizhi@cup.edu.cn (L.-Z. Xiao).

https://doi.org/10.1016/j.petsci.2022.10.020

accurately measure the formations. CPMG-based pulse sequences can greatly reduce the effects of strong dephasing due to the direct or induced magnetic field inhomogeneity, to ensure the precision of each measurement (Xiao et al., 2013). Echo data is acquired with CPMG pulse sequence and the relaxation spectra, including one-dimensional (1D) T_1 and T_2, and two-dimensional (2D) T_1-T_2 and D-T_2, can be constructed with inverse Laplace transformation (ILT) method for subsequent interpretation and application (Xie and Xiao, 2011; Song et al., 2002; Hürlimann and Venkataramanan, 2002). Most importantly, the accuracy and resolution of relaxation spectra are the critical prerequisites for characterizing pore structure, permeability, viscosity and conducting fluid identification.

Generally, the signal response equation of 1D/2D NMR measurements can attribute to the Fredholm integral equation of the first kind, which is a serious ill-conditioned equation with the number of solutions far less than the number of equations, and there is no referable analytical solution. Moreover, the inversion process is very sensitive to noise, and a small disturbance of noise will cause the deviation of the result. So far, the ILT method can be divided into two parts: one is the singular value decomposition (SVD) method based on iteration idea and Bulter-Reeds-Dawsons (BRD) method based on regularization theory (Prammer, 1994; Butler et al., 1981). However, in order to improve the sparsity while maintain the smoothness of relaxation spectra, regularization methods are widely used for practical data processing (for example, T_2 spectra converted into pseudo capillary pressure curve, and etc.). In this idea, a regularization term is added into the objective function and has a constraint on the solutions.

The published literatures on NMR data inversion methods based on regularization theory can mainly divide into four categories: l_2 regularization, l_1 regularization, maximum entropy regularization and double-parameter regularization. l_2 regularization is a method that considers the l_2 norm of the solution as a constraint to solve the objective function, and mainly ensure the smoothness of the solution. Boriga et al. proposed a uniform penalty function to constrain the inversion solution (Borgia et al., 2000), and change the regularization parameter in the inversion process. This method can fit the sharp peaks of T_2 spectra, but may not be converged. Venkataramann et al. and Song et al. used the l_2 norm as the penalty function term, and solved the objective function with BRD method, to obtain the 2D NMR D-T_2 and T_1-T_2 relaxation spectra (Hürlimann and Venkataramanan, 2002; Song et al., 2002). Moreover, the l_2 problem can be solved by Levenberg Marquard (LM) method. Zou et al., reconstructed the objective function combining mixed l_1/l_2 residual term with l_2 regularization term, which was solved by LM method (Zou et al., 2018), and verified the effectiveness of this method for inverting 1D T_2 spectra and 2D D-T_2 spectra. Jin et al. employed the integral transformation method to extract a priori information from the NMR raw echo data, which is used to reconstruct the residual term of the objective function, leading to the improved accuracy of quantitative identification of the bound water (Jin et al., 2019). The regularization term is based on l_2 norm and solved with the BRD method. l_1 regularization is a method that considers the l_1 norm of the solution as a constraint to solve the objective function, and fully considers the sparsity of the solution. Zhou et al. proposed a fast threshold iteration method to solve the objective function based on l_1 regularization constraint, to improve the resolution of the T_1-T_2 relaxation spectra (Zhou et al., 2017). Reci et al. developed a method combining primal-dual with mixed gradient, to solve l_1 regularization problem, and concluded that the proposed method is superior to the traditional methods, such as the BRD and SVD method (Reci et al., 2017). Guo et al. proposed a double-objective function and corresponding optimization method (Guo et al., 2019), in which l_1 regularization is used to solve the first objective function. The solution of l_1 problem was then considered as the initial input to iteratively search the optimal solution with conjugate gradient (CG) method, leading to a good noise resistance and improved resolution of relaxation spectra. Maximum entropy regularization method also considered the sparsity of the solution. Chouzenoux et al. firstly employed Shannon entropy as the penalty function (Chouzenoux et al., 2010), and solved the objective function with Newton method, leading to better sparsity of T_1-T_2 relaxation spectra. Considering the abnormal construction of short relaxation component in the inverted spectra when Shannon entropy method was used, Zou et al. suggested an improved Shannon entropy as the penalty function and solved it with the LM method (Zou et al., 2015). The double-parameter regularization is the combination of l_2 and l_1 regularization or maximum entropy, which considers both the smoothness and sparsity of solution. Berman et al. suggested that l_1 norm and l_2 norm could be introduced as two penalty functions constrained on the solution (Berman et al., 2013), and the objective function was solved with primal-dual interior point method, leading to stable and sparse 1D relaxation spectra. Guo et al. suggested that l_2 norm and Shannon entropy can be used as two penalty terms, which could be solved with the LM method (Guo et al., 2018). Numerical simulation and rock data processing verified the effectiveness of this method.

To overcome the selection of regularization parameters, methods based on the iteration idea are developed. Prammer et al. proposed truncated singular value decomposition (TSVD) method for inverting NMR echo data at first (Prammer, 1994). Since then, many researchers improved TSVD method. Tan et al. proposed LSQR-TSVD hybrid method for inverting 2D NMR relaxation spectra, in which an initial guess of solutions from LSQR is input into the TSVD process to obtain more precise spectra than that by solely using traditional TSVD methods (Tan et al., 2012). Su et al., demonstrated an inversion method worked on 2D spectra by combining L-curve and LSQR method (Su et al., 2016), in which a suitable iteration scheme can be selected for the inversion process. Ge et al. proposed a method combining TSVD with parallel particle swarm optimization algorithm to achieve NMR inversion (Ge et al., 2016).

Furthermore, using machine learning method to obtain NMR relaxation spectra is an inspired and effective inversion method. Wang et al. proposed a new inversion method based on sparse Bayesian clustering, in which the solution of l_2 problem was considered as a priori condition, leading to an improved resolution (Wang et al., 2017). This method was employed for inverting T_1-T_2 relaxation spectra, which only required a few TW sampling points and had the performance with noise adaptivity. Parasram et al. used the artificial neural network method to learn the synthetic echo data, and used the trained model to directly invert the echo data, which improved the accuracy of quantitative identification of free fluid components (Parasram et al., 2021). However, this method required large number of prior simulation data sets for model training, which is very time-consuming. It is worth mentioning that the accuracy of inversion results and the resolution of the spectra can also be improved by suppressing the noise characteristics with denoising methods. The published NMR denoise methods include wavelet threshold method (Xie et al., 2015; Ge et al., 2015), morphological method (Gao et al., 2020), cosine transform method (Gu et al., 2021) and dictionary learning method (Luo et al., 2022), which are not described here.

As mentioned above, each method has its special advantage, but explicit or implicit parameter selection or adjustment will finally affect the inversion results. In practical applications, the one-dimensional and multi-dimensional NMR relaxation spectra should have the following properties: (1) the spectra need to be sparse enough, which can effectively identify the fluid and accurately calculate the relative content of the fluid components; (2) the spectra need to maintain smoothness or stability, which can effectively reflect the continuous distribution of fluid in the rock pores and characterize the pore structure. However, the two properties are normally difficult to maintain at the same time (either too sparse or too smooth). The probability of artificial peaks increases with the complexity of fluid components and lower SNRs, because traditional methods do not effectively address the sparse and redundant characteristics of relaxation spectra in the inversion process. In the work of NMR spectroscopy reconstruction, Qu et al. proposed a method to reconstruct the spectra based on the low-rank property of undersampled free induction decay signals (Qu et al., 2015). The signal property is fully utilized to recover the undersampled NMR signals with high quality, and the spectra after Fourier transform can maintain the Lorentz morphology very well. Inspired by the work of Qu et al., we sincerely consider that this idea can be applied to the construction of low-field NMR relaxation spectra. With the introduction of low-rank and sparsity property, high quality relaxation spectra can be obtained.

In this paper, we propose an inversion method based on non-negative low-rank and sparsity constraints, to construct the objective function with two regularization terms, and solve the objective function using the alternating direction method of multiples (ADMM) method. Numerical simulations are conducted on synthetic echo data at different signal-to-noise ratios (SNRs), to optimize the desirable regularization parameters and verify the feasibility and effectiveness of proposed method. Then, practical NMR experiments on fluids and artificial sandstone samples are conducted and analyzed, which validates the robustness and reliability of proposed method. Simulations and experiments demonstrate that, proposed method has unique advantages for improving the resolution of spectra and enhancing the capability of fluid quantitative identification.

2. Methodology

2.1. 1D and 2D NMR signal responses

For unconventional oil and gas reservoirs exploration, especially for shale reservoirs, 1D T_2 and 2D T_1-T_2 pulse sequences based on CPMG are normally employed for NMR signal acquisition. The inverted NMR spectra can be used for quantitative evaluation of pore structure, fluid mobility, fluid properties and etc (Zhao et al., 2021; Liu et al., 2021). Therefore, this study mainly focuses on the construction of 1D T_2 and 2D T_1-T_2 relaxation spectra with proposed method.

The spin echo data is subject to the multi-exponential decay model (Coates et al., 1999). When CPMG pulse sequence is used, the signal response of 1D T_2 measurement can be expressed by the following Eq. (1):

$$b(t) = \int f(T_2)\exp(-t/T_2)\mathrm{d}T_2 + \varepsilon \tag{1}$$

Here, $b(t)$ is the measured signal amplitude at t moment. The process of solving $f(T_2)$ is the inverse Laplace transformation. However, continuous $f(T_2)$ cannot be directly obtained. Therefore, the relaxation time must be discretized into a vector at first and the upper and lower boundaries need to be defined. It is assumed that all the T_2 relaxation times in decayed signal will not be exceeded over pre-selected boundaries. The discrete form of Eq. (1) can be written as:

$$b_k = \sum_{T_{2,min}}^{T_{2,max}} f(T_{2,j})\exp\left(-\frac{t_k}{T_{2,j}}\right) + \varepsilon_k \tag{2}$$

Here, $j = 1, 2, \cdots, n$, n is the number of discrete relaxation time; $k = 1, 2, \cdots, m$, m is the echo number; t_k is acquisition time and is two times of echo spacing TE (components with relaxation time less than TE will not be detected in NMR experiments); b_k is the amplitude of k-th echo; ε_k is the noise level of k-th echo; $T_{2,j}$ is the j-th component of preselected relaxation times and $f(T_{2,j})$ is corresponding amplitude.

Similarly, the signal response equation of 2D T_1-T_2 can be expressed as the integral Eq. (3):

$$b(t,TW) = \iint f(T_1,T_2)\left(1-2\exp\left(-\frac{TW}{T_1}\right)\right)\exp\left(-\frac{t}{T_2}\right)\mathrm{d}T_1\mathrm{d}T_2 + \varepsilon \tag{3}$$

The discrete form of Eq. (3) is:

$$b_{i,j} = \sum_{m=1}^{m=m'}\sum_{n=1}^{n=n'} f_{m,n}(T_1,T_2)\left(1-2\exp\left(-\frac{TW_i}{T_{1,m}}\right)\right)\exp\left(-\frac{t_j}{T_{2,n}}\right) + \varepsilon_{i,j} \tag{4}$$

Here, $m = 1, 2, \cdots, m'$, m' is the number of discrete component of T_1 relaxation time; $n = 1, 2, \cdots, n'$, n' is the number of discrete component of T_2 relaxation time; TW_i is the waiting time; $f_{m,n}(T_1,T_2)$ is the amplitude of 2D T_1-T_2 relaxation spectra.

2.2. Problem description

Eqs. (2) and (4) are discrete forms of NMR signal response, and the amplitude of each echo is contributed from all relaxation components. Therefore, Eqs. (2) and (4) can be written as a matrix form:

$$\boldsymbol{b} = \boldsymbol{Kf} + \boldsymbol{n} \tag{5}$$

Here, $\boldsymbol{b}$ is the vector of signal amplitude; $\boldsymbol{K}$ is the known kernel matrix. When T_2 measurement is conducted, $K_{k\times j} = \exp(-t_k/T_{2,j})$. When T_1-T_2 measurement is conducted, $K_{ij\times mn} = \left(1-2\exp\left(-\frac{TW_i}{T_{1,m}}\right)\right)\otimes\exp\left(-\frac{t_j}{T_{2,n}}\right)$ and symbol $\otimes$ means tensor product. $\boldsymbol{n}$ is corresponding noise.

In Eq. (5), $\boldsymbol{f}$ is the solution or spectra and must be non-negative. Then, Eq. (5) can be converted into an optimization problem:

$$\boldsymbol{f} = \underset{\boldsymbol{f}\geq 0}{\mathrm{argmin}}\|\boldsymbol{Kf}-\boldsymbol{b}\|_2^2 \ \ s.t., \ \boldsymbol{Kf} = \boldsymbol{b} \tag{6}$$

It is obvious that Eq. (6) is a non-negative least square solution problem. In order to avoid over-fitting of the solution, l_2 regularization constraint is usually imposed on $\boldsymbol{f}$:

$$\boldsymbol{f} = \underset{\boldsymbol{f}\geq 0}{\mathrm{argmin}}\|\boldsymbol{Kf}-\boldsymbol{b}\|_2^2 + \alpha\|\boldsymbol{f}\|_2^2 \quad s.t., \ \boldsymbol{Kf} = \boldsymbol{b} \tag{7}$$

Eq. (7) can be solved by using BRD or LM method as aforementioned. In addition, l_2 regularization term can be modified by using l_1 restraints to improve the sparsity of spectra but may result in under-smoothness and produce artificial peaks. Therefore, double-parameter regularization methods are proposed and suggested to balance smoothness and sparsity of spectra (Berman et al., 2013; Guo et al., 2018). However, it is generally considered that the points in the spectra are independent of each other, leading to irregular shape and artificial peaks of spectra, even though experiments are conducted with high SNRs. This situation will be explained in details later.

In order to fully extract the effective information and eliminate the redundant information of spectra with improved resolution and accuracy, non-negative low-rank and sparsity restraints are added into the objective function. Then Eq. (6) can be converted as followed problem:

$$\boldsymbol{f} = \underset{\boldsymbol{f}\geq 0}{\operatorname{argmin}} \|\Gamma \boldsymbol{f}\|_* + \lambda_1 \|\boldsymbol{f}\|_1 + \lambda_2 \|\boldsymbol{Kf} - \boldsymbol{b}\|_2^2$$

$$\boldsymbol{s.t.}\ \ \boldsymbol{Kf} = \boldsymbol{b} \tag{8}$$

Here, λ_1 and λ_2 are regularization parameters; $\|\bullet\|_*$ is the nuclear norm, which is the sum of singular value of a matrix; Γ is the operator to convert a vector into a matrix. In 1D inversion problem, Γ could be Hankel matrix operator (Qu et al., 2015). In 2D inversion problem, $\Gamma \boldsymbol{f}$ is 2D relaxation spectra. For example, $\boldsymbol{f}$ is a vector with length of 2500, and $\Gamma \boldsymbol{f}$ is the 2D spectra with size of 50*50. In Eq. (8), the first term constrains the low-rank property of the spectra, the second term constrains the sparsity of the spectra, and the third term constrains the accuracy of the spectra and reflects the noise disturbance of the solution. Therefore, the optimization problem is converted into solving the low-rank and sparse 1D or 2D relaxation spectra.

2.3. Algorithm description based on non-negative low-rank and sparsity restraint

According to Eq. (8), optimized variable $\boldsymbol{f}$ is appeared in nuclear norm term, l_1 norm term and residual norm term, simultaneously. The objective function can not be directly solved so that ADMM can be applied to convert objective function into three subproblems, which can be solved independently (Qu et al., 2015; Lu et al., 2018).

To avoid the confusion of variable $\boldsymbol{f}$ in subproblems, auxiliary variables $\boldsymbol{H}$, $\boldsymbol{h}$ and $\boldsymbol{e}$, and Lagrange multipliers $\boldsymbol{X}_1$, $\boldsymbol{X}_2$ and $\boldsymbol{X}_3$ are introduced into objective function. Therefore, the problem of Eq. (8) can be rewritten as a new form:

$$\boldsymbol{f} = \underset{\boldsymbol{f}\geq 0}{\operatorname{argmin}} \|\Gamma \boldsymbol{f}\|_* + \lambda_1 \|\boldsymbol{f}\|_1 + \lambda_2 \|\boldsymbol{Kf} - \boldsymbol{b}\|_2^2$$

$$\boldsymbol{s.t.}\ \ \boldsymbol{b} = \boldsymbol{Kf} + \boldsymbol{e},\ \Gamma \boldsymbol{f} = \boldsymbol{H},\ \boldsymbol{f} = \boldsymbol{h} \tag{9}$$

With the augmented Lagrange function, Eq. (9) can be converted into an optimization problem in a non-restraint form:

$$\begin{aligned}\{\boldsymbol{H},\boldsymbol{h},\boldsymbol{e}\} &= \operatorname{argmin} \mathscr{L}(\boldsymbol{H},\boldsymbol{h},\boldsymbol{e},\boldsymbol{X}_1,\boldsymbol{X}_2,\boldsymbol{X}_3,\mu)\\ &= \|\boldsymbol{H}\|_* + \lambda_1\|\boldsymbol{h}\|_1 + \lambda_2\|\boldsymbol{e}\|_2^2 + \langle \boldsymbol{X}_2, \Gamma\boldsymbol{f} - \boldsymbol{H}\rangle + \langle \boldsymbol{X}_3, \boldsymbol{f} - \boldsymbol{h}\rangle\\ &\quad + \langle \boldsymbol{X}_1, \boldsymbol{b} - \boldsymbol{Kf} - \boldsymbol{e}\rangle + \frac{\mu}{2}\left(\left\|\Gamma\boldsymbol{f} - \boldsymbol{H} + \frac{\boldsymbol{X}_2}{\mu}\right\|_F^2\right.\\ &\quad \left. + \left\|\boldsymbol{f} - \boldsymbol{h} + \frac{\boldsymbol{X}_3}{\mu}\right\|_F^2 + \left\|\boldsymbol{b} - \boldsymbol{Kf} - \boldsymbol{e} + \frac{\boldsymbol{X}_1}{\mu}\right\|_F^2\right)\end{aligned} \tag{10}$$

Here, $<\bullet,\bullet>$ is inner product, μ is the dual variable which is acted as the step-size controller in each iteration. By alternatively solving and updating variables $\boldsymbol{H}$, $\boldsymbol{h}$ and $\boldsymbol{e}$, $\mathscr{L}(\boldsymbol{H},\boldsymbol{h},\boldsymbol{e},\boldsymbol{X}_1,\boldsymbol{X}_2,\boldsymbol{X}_3,\mu)$ will be optimized.

The optimization of three subproblems can be solved and iteratively updated as followed scheme:

1. Fixing other variables and updating $\boldsymbol{H}$:

$$\boldsymbol{H} = \operatorname{argmin}\|\boldsymbol{H}\|_* + \left\|\Gamma\boldsymbol{f} - \boldsymbol{H} + \frac{\boldsymbol{X}_2}{\mu}\right\|_F^2 \tag{11}$$

where, the solution of Eq. (11) is $\Theta_{\frac{1}{\mu}}\left(\boldsymbol{H} + \frac{\boldsymbol{X}_2}{\mu}\right)$, and Θ is the minimum operator of nuclear norm, which can be obtained with singular value thresholding (SVT) method (Cai et al., 2010).

2. Fixing other variables and updating $\boldsymbol{h}$:

$$\boldsymbol{h} = \operatorname{argmin}\lambda_1\|\boldsymbol{h}\|_1 + \left\|\boldsymbol{f} - \boldsymbol{h} + \frac{\boldsymbol{X}_3}{\mu}\right\|_F^2 \tag{12}$$

where, the solution of Eq. (12) is $\boldsymbol{\Psi}_{\frac{\lambda_1}{\mu}}\left(\left(\boldsymbol{h} + \frac{\boldsymbol{X}_3}{\mu}\right)\right)$, and $\boldsymbol{\Psi}$ is the minimum operator of l_1 norm, which can be obtained with shrinking thresholding (ST) method (Lin et al., 2010).

3. Fixing other variables and updating $\boldsymbol{e}$:

$$\boldsymbol{e} = \operatorname{argmin}\lambda_2\|\boldsymbol{e}\|_2^2 + \left\|\boldsymbol{b} - \boldsymbol{Kf} - \boldsymbol{e} + \frac{\boldsymbol{X}_1}{\mu}\right\|_F^2 \tag{13}$$

where, the solution of Eq. (13) is $\boldsymbol{\Omega}_{\frac{\lambda_2}{\mu}}\left(\left(\boldsymbol{b} - \boldsymbol{Kf} + \frac{\boldsymbol{X}_1}{\mu}\right)\right)$, and $\boldsymbol{\Omega}$ is the minimum operator of l_2 norm. Its approximate solution is $\mu \times \left(\boldsymbol{b} - \boldsymbol{Kf} + \frac{\boldsymbol{X}_1}{\mu}\right) / (\lambda_2 + \mu)$ (Zhuang et al., 2012).

4. Fixing other variables and updating $\boldsymbol{f}$:

$$\boldsymbol{f} = \left(\boldsymbol{K}^{\mathrm{T}}\boldsymbol{K} + 2\boldsymbol{I}\right)\left[\boldsymbol{K}^{\mathrm{T}}(\boldsymbol{b} - \boldsymbol{e} + \boldsymbol{X}_1/\mu) - \left(\Gamma^{-1}\boldsymbol{X}_2 + \boldsymbol{X}_3\right)/\mu + \boldsymbol{h} + \Gamma^{-1}\boldsymbol{H}\right] \tag{14}$$

where Γ^{-1} is the operator for converting 2D matrix into 1D vector.

In a summary, the workflow for solving equations with ADMM is illustrated in Table 1.

3. Simulations

3.1. One-dimensional T_2 relaxation spectra

3.1.1. Model construction

The relaxation spectra are subject to the Gaussian distribution (Prange and Song, 2009; Wang et al., 2017). In order to verify the effectiveness of proposed method, synthetic echo data based on Gaussian distribution or random walk of particles in digital rocks is used as forward modeling for inversion process. For simplicity, we conduct forward modeling based on Gaussian distribution to construct raw echo data. The establishment of forward modeling includes five steps: 1. using Gaussian function to determine the location of peaks and the morphology of the fluid components; 2. simulating pulse sequence parameters, such as echo spacing, echo number and other acquisition parameters; 3. calculating the kernel function of Laplace transformation matrix according to the acquisition parameters and the discrete relaxation components; 4. calculating the noiseless echo data according to the spectra amplitude and kernel matrix, and then adding noise. Finally, the inversion method can be verified with synthetic NMR echo data. In this subsection, 1D T_2 inversion is analyzed at first.

For 1D inversion, we build two bimodal relaxation spectra with the same fluid components but different relative content to simulate the bound water (BW) and movable oil (MO) in rock pores, as demonstrated in Fig. 1. The relaxation time of BW is 8 ms and MO is

Table 1
The proposed algorithm and workflow for the acquisition of optimal solutions with low-rank and sparsity restraint.

Optimization Algorithm based on Low-rank and Sparsity Restraint
Input: measured signal b; kernel matrix A; regularization parameter λ_1, λ_2; step-size μ; iteration number t.
Initialization: Tol $\varepsilon = 10^{-6}$; $\boldsymbol{f}_0 = \boldsymbol{h}_0 = \boldsymbol{e}_0 = \boldsymbol{X}_1 = \boldsymbol{X}_3 = 0$; $\boldsymbol{H}= \boldsymbol{X}_2 = 0$; $\mu_0 = 0.01$; $\mu_{max} = 10^5$; $t = 0$; $\xi_0 = 1.01$.
1: while $\max\left(\|\boldsymbol{f} - \Gamma^{-1}\boldsymbol{H}\|_{\boldsymbol{F}}^{\boldsymbol{2}}, \|\boldsymbol{f} - \boldsymbol{h}\|_{\boldsymbol{F}}^{\boldsymbol{2}}, \|\boldsymbol{b} - \boldsymbol{K}\boldsymbol{f} - \boldsymbol{e}\|_{\boldsymbol{F}}^{\boldsymbol{2}}\right) > \varepsilon$ **do**
2: Fixing other variables and updating $\boldsymbol{H}$ of (11) with SVT operator;
3: Fixing other variables and updating $\boldsymbol{h}$ of (12) with ST operator;
4: Fixing other variables and updating $\boldsymbol{e}$ of (13) with l_2 minimization operator;
5: Updating $\boldsymbol{f}$ with Eq. (14): $\boldsymbol{f} = (\boldsymbol{K}^{\mathrm{T}}\boldsymbol{K} + 2\boldsymbol{I})[\boldsymbol{K}^{\mathrm{T}}(\boldsymbol{b} - \boldsymbol{e} + \boldsymbol{X}_1/\mu) - (\Gamma^{-1}\boldsymbol{X}_2 + \boldsymbol{X}_3)/\mu + \boldsymbol{h} + \Gamma^{-1}\boldsymbol{H}]$
6: Updating Lagrange multipliers as followed:
$\boldsymbol{Y}_{1,t+1} = \boldsymbol{Y}_{1,t} + \mu_t \times (\boldsymbol{b} - \boldsymbol{K}\boldsymbol{f}_{t+1} - \boldsymbol{e}_{t+1})$
$\boldsymbol{Y}_{2,t+1} = \boldsymbol{Y}_{2,t} + \mu_t \times (\boldsymbol{f}_{t+1} - \Gamma^{-1}\boldsymbol{H}_{t+1})$
$\boldsymbol{Y}_{3,t+1} = \boldsymbol{Y}_{3,t} + \mu_t \times (\boldsymbol{f}_{t+1} - \boldsymbol{h}_{t+1})$
7: Updating μ as followed:
$\mu_{t+1} = \min(\mu_{\max}, \xi\mu_t)$, where
$\xi = \begin{cases} \xi_0, \text{ if } \max\left(\left\|\boldsymbol{f} - \Gamma^{-1}\boldsymbol{H}\right\|_{\boldsymbol{F}}^{\boldsymbol{2}}, \|\boldsymbol{f} - \boldsymbol{h}\|_{\boldsymbol{F}}^{\boldsymbol{2}}, \|\boldsymbol{b} - \boldsymbol{K}\boldsymbol{f} - \boldsymbol{e}\|_{\boldsymbol{F}}^{\boldsymbol{2}}\right) < \varepsilon \\ 1, \text{ otherwise} \end{cases}$
8: Updating $t = t + 1$;
9: end while
Output: optimal solution $\boldsymbol{f}$.

150 ms. The total porosity is 10 p.u., and the relative content ratio between BW and MO is 3:2 for model 1 (as demonstrated in Fig. 1(a)) and 2:3 for model 2 (as demonstrated in Fig. 1(b)), respectively. Fig. 1(c) and (d) are forwarding echo data from Fig. 1(a)

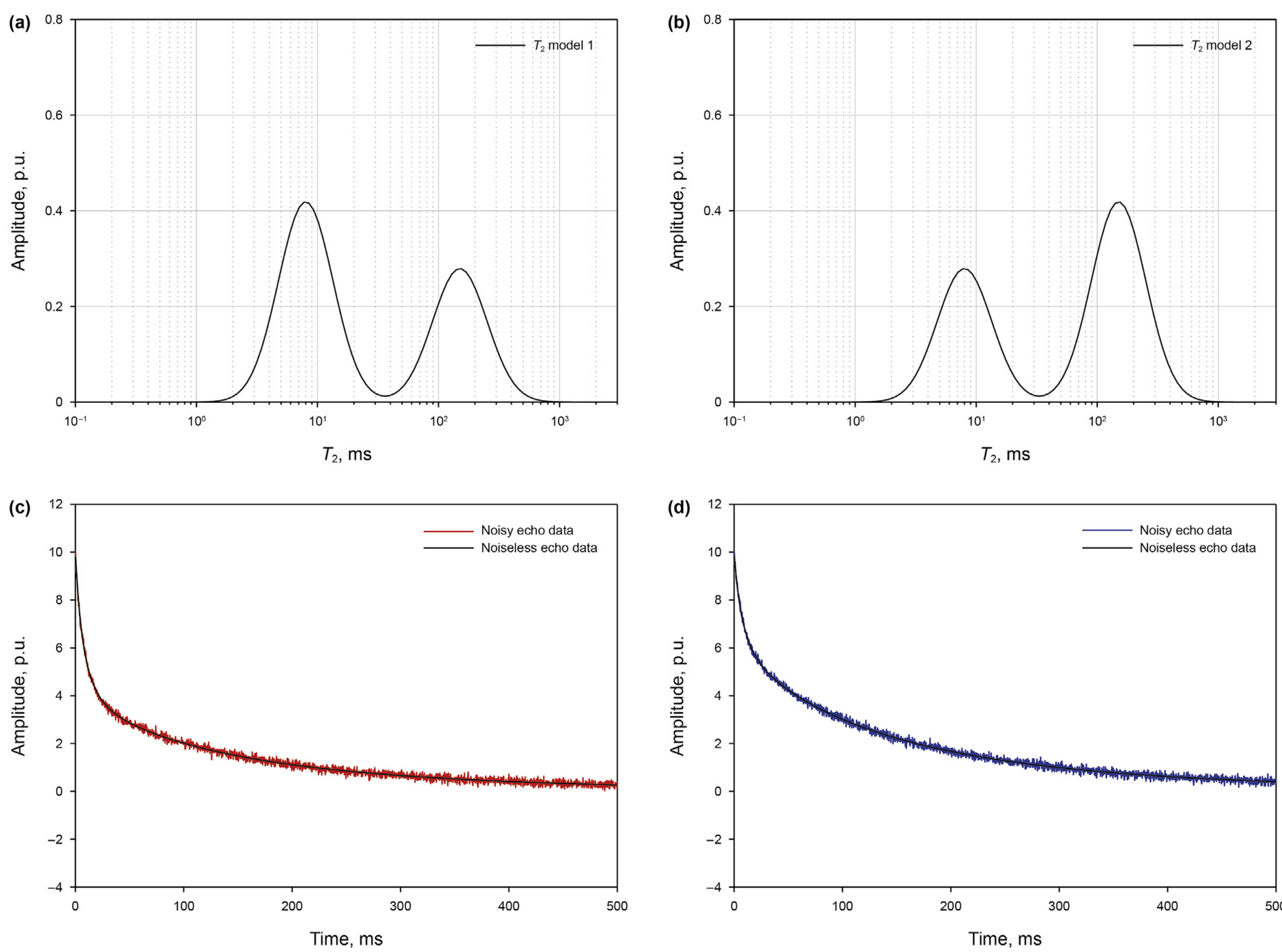

Fig. 1. Bimodal T_2 spectra based on Gaussian distribution and corresponding NMR signal response. (a) bimodal T_2 spectrum with MO dominated; (b) bimodal T_2 spectrum with CBW dominated; (c) and (d) are NMR signals corresponding to (a) and (b), respectively.

and Fig. 1(b) respectively. Considering the enough decay of echo data, echo spacing *TE* is set as 0.2 ms and echo number is set as 2500.

3.1.2. Selection of regularization parameters

The selection of regularization parameters is important for obtaining reliable and precise solutions. However, an optimal selection for double parameters is very difficult. Therefore, we conduct a global search for two regularization parameters and observe the variation of root-mean-square error (RMSE) between models and inversion results. Further works on the optimization of double regularization parameters is undergoing. The interval of λ_1 and λ_2 is set as [0.01 100] and 50 points are logarithmically distributed in this interval. Considering model 1 as an instance, synthetic echo data with different SNR of 100, 50, 20 and 10 is constructed, respectively. The expression of RMSE is as follows:

$$\mathrm{RMSE} = \sqrt{\frac{\sum_{i=1}^{i=N} \left(f\left(\hat{T}_{2i}\right) - f(T_{2i}) \right)^2}{N}} \tag{15}$$

where, $f(\widehat{T_{2i}})$ is the amplitude of the relaxation component in the inverted spectra, and $f(T_{2i})$ is the amplitude of relaxation component in the model.

The calculated RMSE after LRSR inversion process is demonstrated in Fig. 2. With the decrease of SNR, the RMSE of the solution gradually increases, which is reflected in the gradual expansion of the isolines. When the SNR is high, the disturbance of noise to the solution is small, leading to the relatively high value of λ_1 and λ_2. In this situation, spectra can balance the sparsity and smoothness while ensuring the precision and morphology. When SNR is lower than 20, RMSE is gradually decreased. In this situation, λ_1 and λ_2 should be decreased, and λ_2 should lower than λ_1. In order to ensure the sparsity and smoothness, slightly sacrificing the precision of solutions is necessary, which will lead to the increment of RMSE. The yellow dots in Fig. 2 represent the optimal values of regularization parameters λ_1 and λ_2, leading to the lowest RMSE of inversion results. It can be seen that, λ_1 and λ_2 are within the interval of [0.1 10] and the ratio of λ_2/λ_1 is gradually decreased, with the SNRs changed from 100 to 10. The optimal values of regularization parameters λ_1 and λ_2 are illustrated in Table 2.

In the followed works, we will adopt the optimal values of regularization parameters in Table 2.

3.1.3. 1D inversion analysis

To verify the effectiveness of proposed method, inversion results obtained with BRD and LSQR-TSVD methods are considered for the

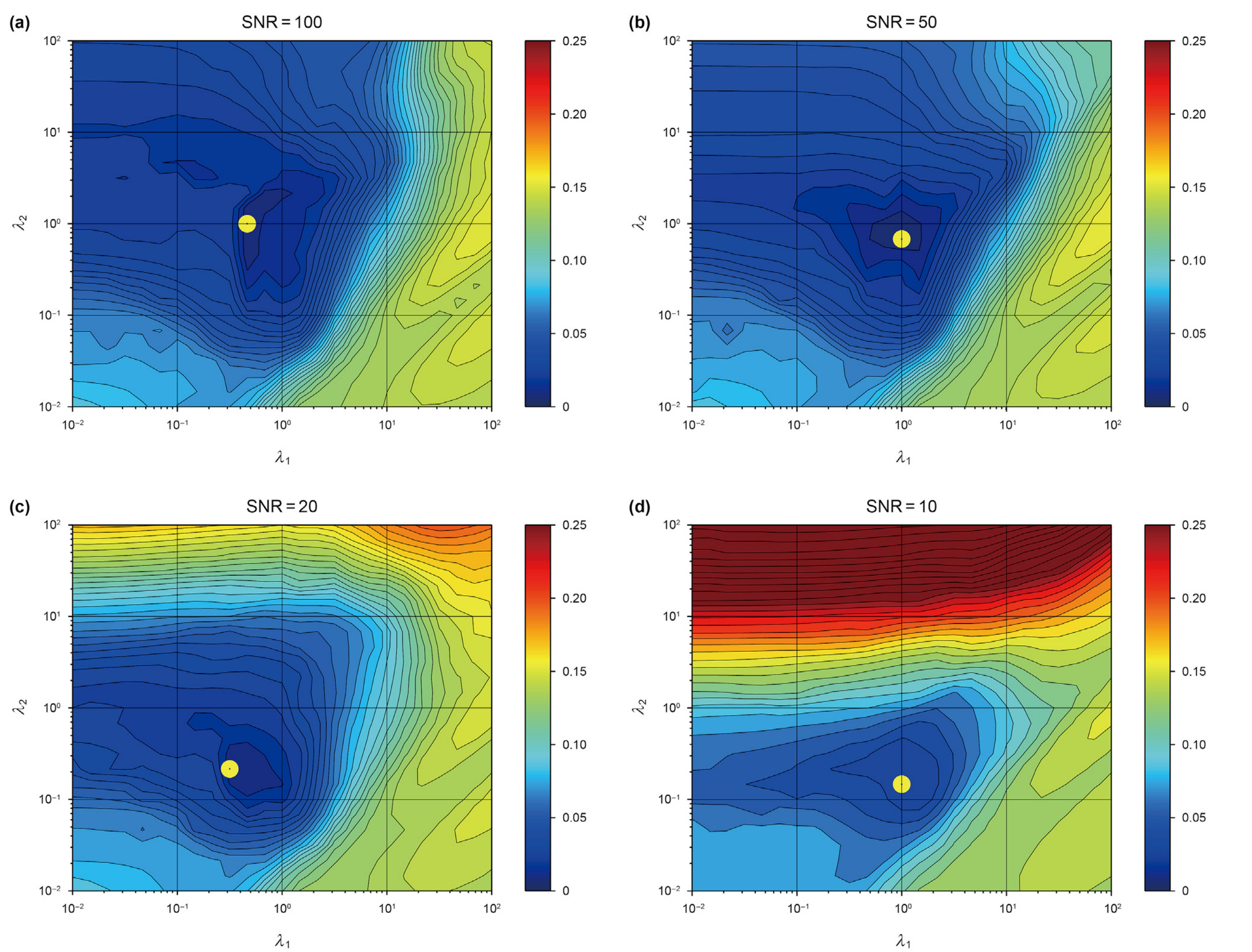

Fig. 2. Variation of RMSE at different SNRs when regularization parameters changed. (a) SNR = 100; (b) SNR = 50; (c) SNR = 20; (d) SNR = 10. The yellow dot demonstrates the minimum RMSE and points out the optimal regularization parameters.

Table 2
Optimal values of regularization parameters for 1D LRSR inversion.

SNRs	λ_1	λ_2	λ_2/λ_1
100	1.24	4.20	3.38
50	0.98	1.38	1.41
20	0.71	0.45	0.63
10	0.65	0.22	0.34

comparison. The RMSE, accumulated porosity and the BW/MO ratio are compared. The S-curve method is adopted for the optimal regularization selection of BRD inversion method. LSQR-TSVD is a hybrid method based on the iteration idea, which has the ability with desirable inversion speed and better resolution. The T_2 spectra of model 1 and model 2 inverted by using BRD, LSQR-TSVD and proposed LRSR methods are demonstrated in Figs. 3 and 4, respectively.

It can be seen from Figs. 3 and 4 that different fluid components can be clearly distinguished at different SNRs. However, the difference between three methods is obvious. At higher SNR (SNR≥50), the inverted spectra are very close to the forwarding models, and high resolution and small RMSE are obtained. When SNR is lower than 20, the inverted spectra are deviated from the forwarding model with increased RMSE. In order to ensure the stability of solutions and avoid artificial relaxation peaks, inverted spectra of BRD method are tended to be smoother, leading to higher RMSE. The reason is that the selection of the optimal regularization parameter reduces the condition number of the matrix, leading to the smoothness. LSQR-TSVD method demonstrates good performance for enhancing the resolution of spectra compared to BRD method. In this method, an initial guess which is calculated by LSQR and input into TSVD to be further solved. Whereas, LRSR demonstrates the best performance due to the introduced low-rank and sparsity restraint. It will enhance the relevance between adjoint points, highlight the effective components and eliminate the artifacts in the spectra during inversion process. In other words, the smoothness and stability can be ensured with low-rank restraint. The resolution can be ensured with sparsity restraint. Quantitative information of porosity, RMSE and BW/MO ratio at different SNRs obtained with these three methods, are illustrated in Table 3. It is indicated that LRSR method is superior than BRD and LSQR-TSVD methods, from the aspects of porosity, RMSE, and fluid quantitative identification.

In order to study the performance of LRSR method on noise resistance, 1000 random simulations are conducted at different SNRs. The T_2 spectra inverted by using LRSR method are compared with that inverted by using BRD and LSQR-TSVD methods. For simplicity, model 1 is used for the probability statistics of porosity, RMSE and BW/MO ratio, which are demonstrated in Fig. 5. It is shown that the inversion results obtained with LRSR method is more close to the model, and have a higher probability distribution around the pre-set values of the model (such as porosity and BW/

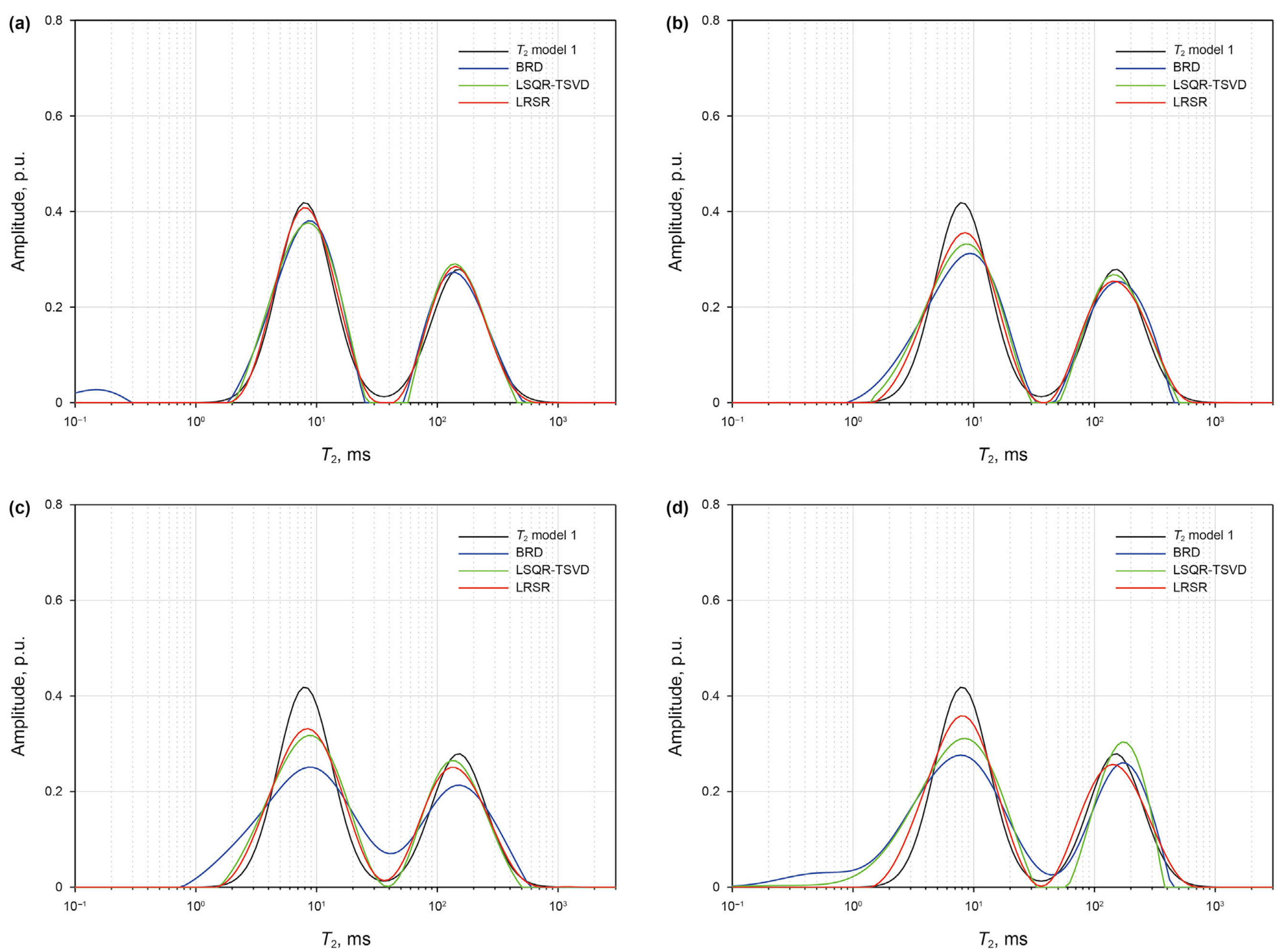

Fig. 3. T_2 spectra inverted by using BRD, LSQR-TSVD and LRSR methods based on model 1 at different SNRs. (a) SNR = 100; (b) SNR = 50; (c) SNR = 20; (d) SNR = 10.

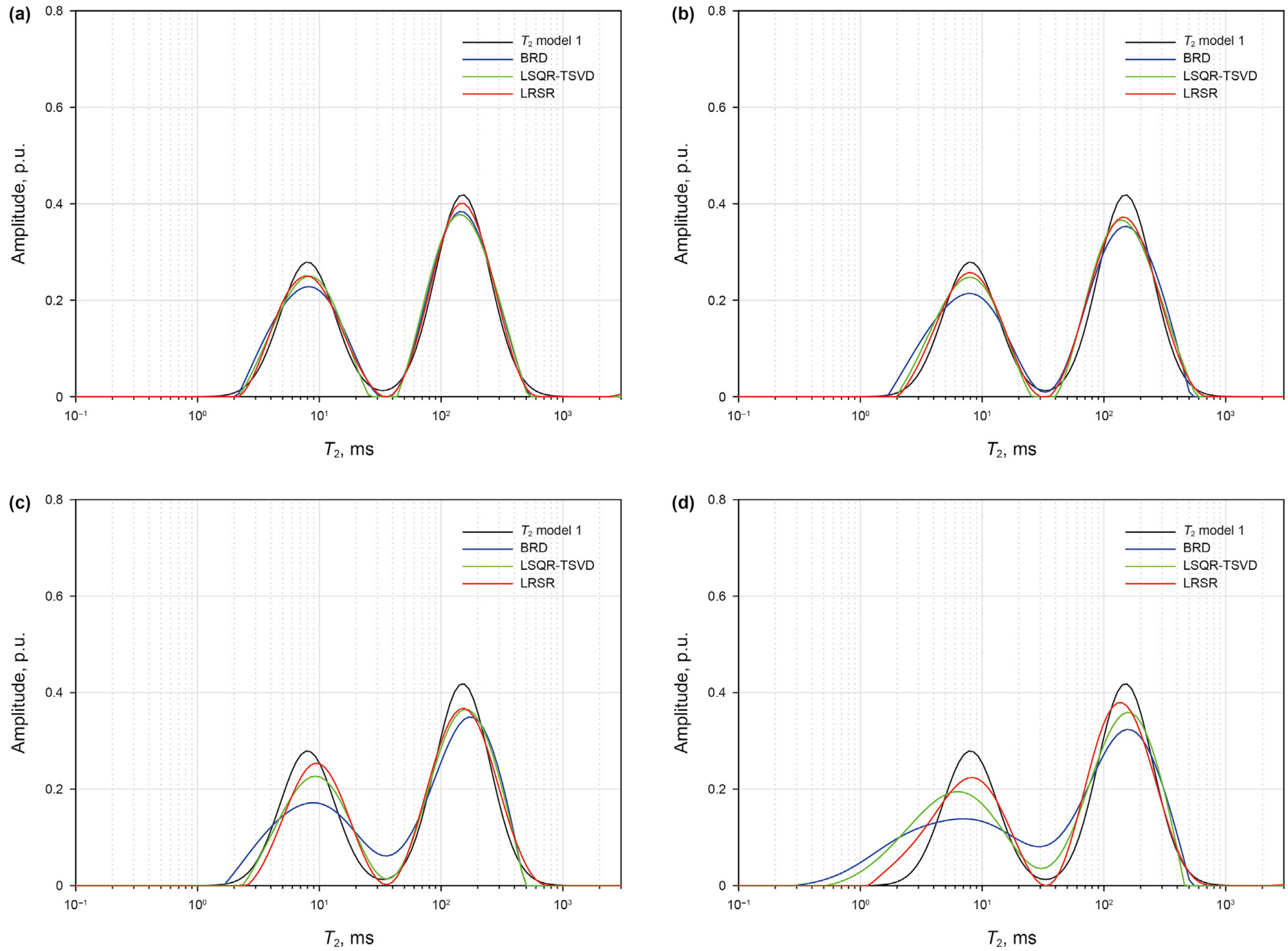

Fig. 4. T_2 spectra inverted by using BRD, LSQR-TSVD and LRSR methods based on model 2 at different SNRs. (a) SNR = 100; (b) SNR = 50; (c) SNR = 20; (d) SNR = 10.

Table 3
Comparison of BRD, LSQR-TSVD and LRSR methods applied on model 1 and model 2 at different SNRs, when optimal regularization parameters selected.

Model 1	BRD				LSQR-TSVD				LRSR			
SNRs	100	50	20	10	100	50	20	10	100	50	20	10
RMSE_1	0.019	0.033	0.043	0.045	0.018	0.0259	0.035	0.039	0.010	0.019	0.025	0.031
Porosity_1	10.335	10.146	10.430	10.662	10.090	10.082	10.344	10.479	10.142	10.070	10.163	10.306
BW/MO_1	1.590	1.582	1.613	1.825	1.548	1.561	1.581	1.811	1.490	1.491	1.534	1.492
Model 2	BRD				LSQR-TSVD				LRSR			
SNRs	100	50	20	10	100	50	20	10	100	50	20	10
RMSE_2	0.015	0.021	0.032	0.050	0.015	0.015	0.025	0.041	0.007	0.013	0.022	0.037
Porosity_2	9.979	10.073	10.089	9.673	9.959	10.023	9.933	9.914	10.029	9.983	10.030	9.910
BW/MO_2	0.667	0.685	0.689	0.732	0.671	0.675	0.685	0.699	0.661	0.666	0.671	0.677

MO ratio). The dispersion of the probability distribution may result from the noise disturbance and randomness. With the decrease of SNR, the RMSE of inversion results using BRD and LSQR-TSVD methods becomes larger, and the ability of fluid identification and quantification also decreases. On the contrary, the LRSR method maintains a relatively stable performance. Table 4 lists the averaged values of 1000 random simulations at different SNRs for BRD, LSQR-TSVD and LRSR methods. The 1D simulation results demonstrate that LRSR method has better noise resistance and is more accurate in porosity calculation and fluid quantitative identification.

The time consumption and memory usage of BRD, LSQR-TSVD and LRSR methods are compared as well. The processor of PC is 2.9 GHz Intel Core i7-10700, and memory storage is 32 GB. Simulation software MATLAB 2021b is used for the computation. Table 5 illustrates the time consumption and memory usage of each inversion method. For 1D NMR inversion, the operation time of LRSR method is slightly larger than that of other methods but has moderate memory usage. The inversion speed should be improved in future work since it is important for real-time NMR logging. Next, we will carry on numerical simulation and analysis of 2D T_1-T_2 spectra.

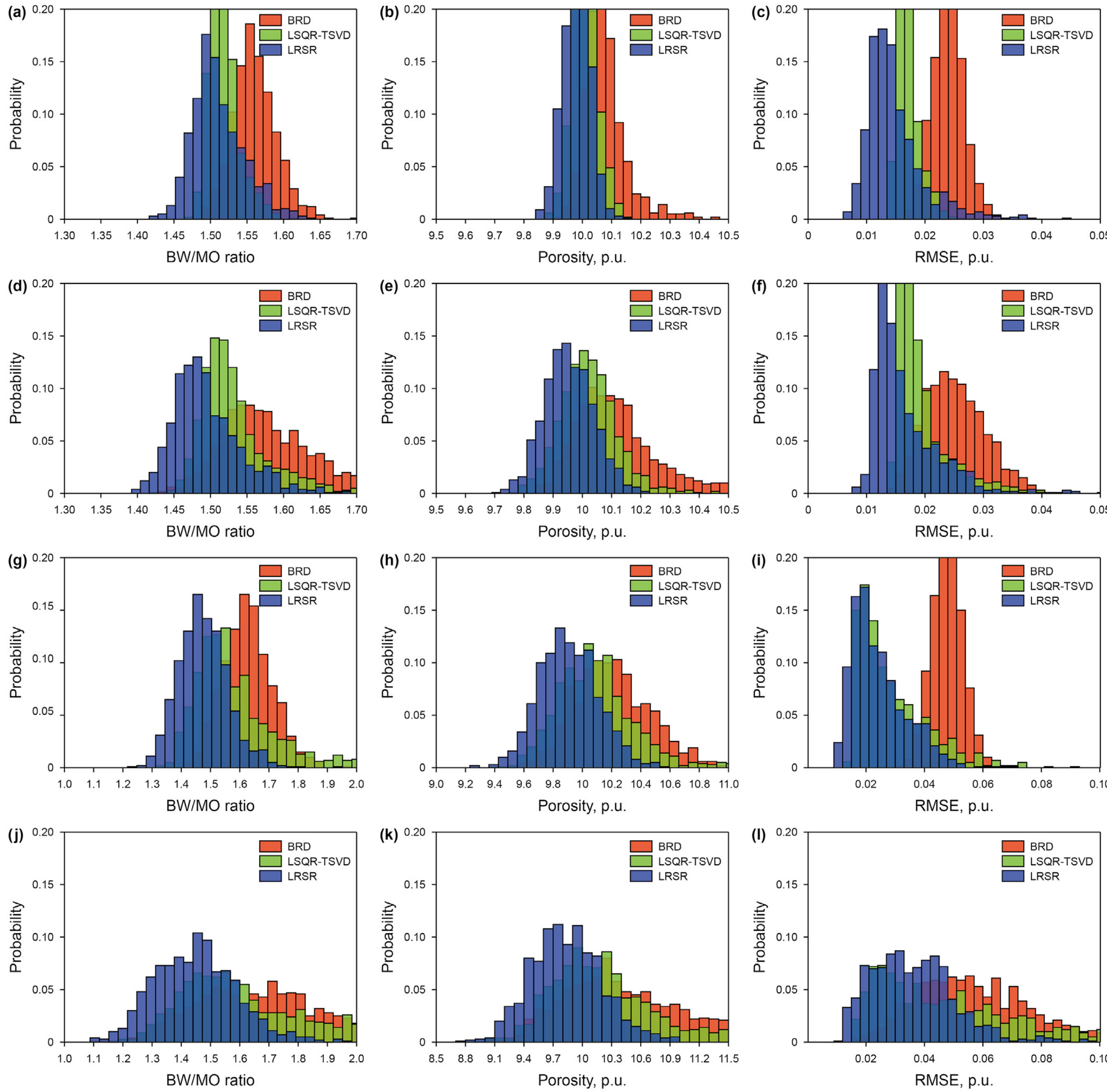

Fig. 5. 1000 random simulations using BRD, LSQR-TSVD and LRSR methods at different SNRs, and model 1 is used as an example for probability statistics. (a)–(c) SNR = 100; (d)–(f) SNR = 50; (g)–(i) SNR = 20; (j)–(l) SNR = 10.

Table 4
Comparison of inversion results obtained by using BRD, LSQR-TSVD and LRSR methods at different SNRs and corresponding averaged values of RMSE, porosity and BW/MO ratio.

Model 1	BRD				LSQR-TSVD				LRSR			
SNRs	100	50	20	10	100	50	20	10	100	50	20	10
RMSE_1	0.024	0.025	0.048	0.057	0.017	0.019	0.029	0.052	0.015	0.017	0.024	0.036
Porosity_1	10.078	10.127	10.208	10.617	10.009	10.022	10.128	10.386	9.981	9.954	9.906	9.841
BW/MO_1	1.561	1.579	1.628	1.736	1.518	1.532	1.583	1.680	1.511	1.496	1.476	1.450
Model 2	BRD				LSQR-TSVD				LRSR			
SNRs	100	50	20	10	100	50	20	10	100	50	20	10
RMSE_2	0.020	0.022	0.0380	0.042	0.016	0.019	0.029	0.050	0.016	0.017	0.025	0.036
Porosity_2	10.066	10.128	10.185	10.318	10.008	10.055	10.180	10.418	9.979	9.959	9.904	9.850
BW/MO_2	0.684	0.695	0.712	0.732	0.667	0.680	0.717	0.780	0.673	0.660	0.649	0.638

Table 5
Time consumption and memory usage.

Name	BRD	LSQR-TSVD	LRSR
Time, s	0.030	0.416	0.503
Memory, MB	3.003	5.895	4.344

3.2. Two-dimensional T_1-T_2 spectra

3.2.1. Model construction

For the forwarding model of 2D T_1-T_2 relaxation spectra, three fluid components are constructed, including bound water (BW), movable oil (MO) and movable water (MW). The T_1 relaxation time of three components is 5 ms, 30 ms, and 200 ms, respectively. The T_2 relaxation time of three components is 4 ms, 25 ms, and 150 ms, respectively. The T_1/T_2 ratio is within the interval of [1, 2]. For simplicity, the total porosity of model is set as 12 p.u., and the proportion of three components is set as 4 : 4: 4. Based on this model, the acquisition parameters, polarization time *TW* is set as [5000; 4000; 2000; 1000; 800; 500; 250; 125; 100; 50; 25; 15; 10; 8; 6; 5; 4; 2; 1; 0.1] ms, echo spacing *TE* is set as 0.2 ms and echo number *NE* is set as 2500.

The T_1-T_2 relaxation spectra and corresponding NMR signals based on forwarding model and acquisition parameters are demonstrated in Fig. 6(a) and (b), respectively. It can be seen from Fig. 6 that the NMR echo data acquired by 2D T_1-T_2 pulse sequence is essentially a 1D time-domain signal, and the T_1-T_2 relaxation spectra is obtained by inverse Laplace transformation. The projection of T_1-T_2 relaxation spectra along the T_2 direction is T_2 spectrum, and the projection along the T_1 direction is T_1 spectrum. Both T_1 and T_2 relaxation times jointly determine the characteristics of 2D T_1-T_2 relaxation spectra of the detected samples. In the 2D spectra, three kinds of fluid components can be clearly identified, and the area of the corresponding local peak is the absolute content of the fluid component, which can be quantitatively calculated.

Table 7
Optimal values of regularization parameters for inverting 2D T_1-T_2 correlation spectra.

SNRs	λ_1	λ_2	λ_2/λ_1
100	3.12	5.10	1.63
50	3.00	2.50	0.83
20	2.40	0.80	0.33
10	1.60	0.11	0.07

3.2.2. 2D inversion analysis

Different from 1D inversion, the amount of 2D NMR echo data is largely increased, leading to an increment in acquisition time and a serious reduction of data processing speed. By compiling pulse sequence (Du et al., 2020) and data compression before inversion process (Mitchell et al., 2012), the acquisition time can be effectively reduced and the inversion speed may be increased. Therefore, for 2D NMR echo data, we use the truncated singular value compression (SVDc) method to compress the 2D echo data at first, and then use the BRD and LRSR methods to invert the compressed

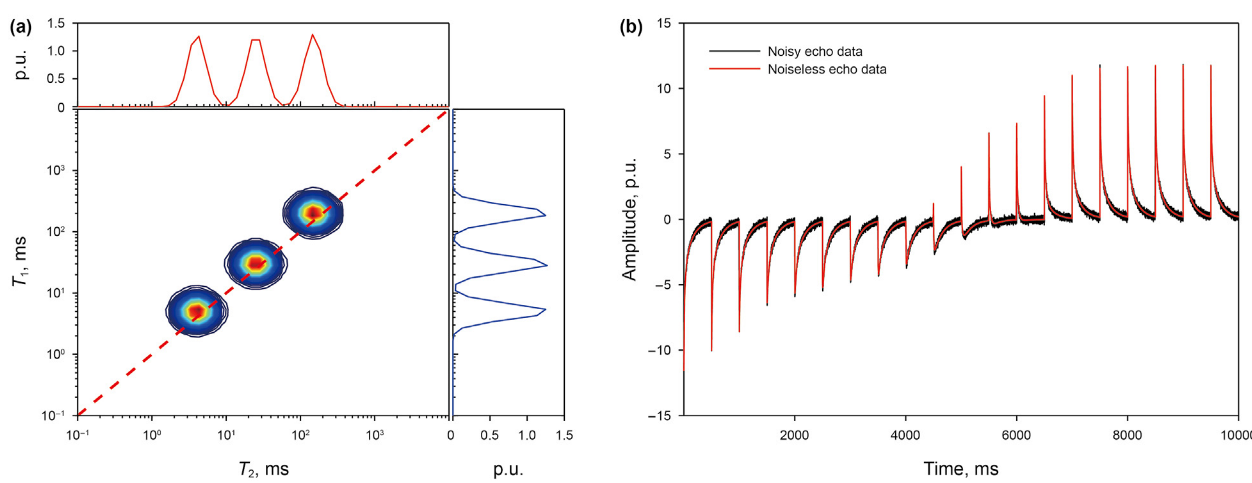

Fig. 6. Forwarding model of T_1-T_2 relaxation spectra and synthetic NMR signals. (a) T_1-T_2 correlated spectra constructed from bound water (BW), movable oil (MO) and movable water (MW); (b) synthetic echo data of three fluid components.

Table 6
Inversion results of 2D T_1-T_2 data by using BRD, LSQR-TSVD and LRSR methods with different SNRs.

SNRs	100	50	20	10
BRD				
RMSE (p.u.)	0.017	0.020	0.024	0.032
Porosity (p.u.)	12.24	12.33	12.46	12.94
BW:MO:MW	4.03:4.08:3.96	3.87:3.93:3.98	3.66:3.55:4.15	3.20:3.61:4.06
LSQR-TSVD				
RMSE (p.u.)	0.015	0.021	0.025	0.028
Porosity (p.u.)	12.20	12.24	12.41	12.78
BW:MO:MW	3.55:3.68:4.04	3.58:3.71:4.03	3.25:3.68:4.08	2.88:3.56:4.14
LRSR				
RMSE (p.u.)	0.012	0.016	0.018	0.024
Porosity (p.u.)	12.07	12.12	12.21	12.51
BW:MO:MW	3.97:4.01:3.98	3.89:4.05:4.08	3.76:4.03:4.11	3.62:4.14:4.08

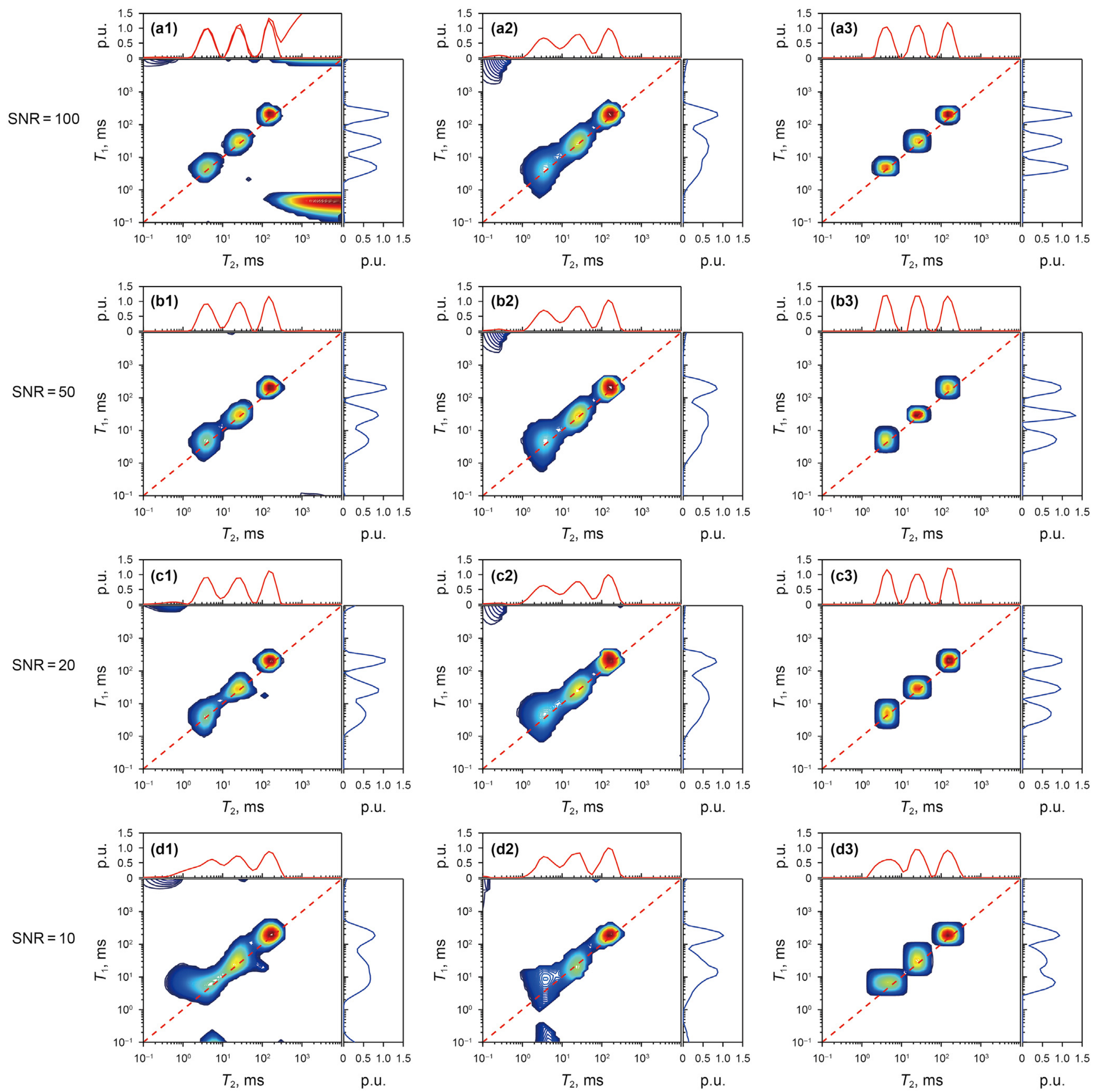

Fig. 7. T_1-T_2 relaxation spectra inverted by using different methods at different SNRs. (a1)~(d1) demonstrate the T_1-T_2 spectra inverted by using the BRD method. (a2)~(d2) demonstrate the T_1-T_2 spectra inverted by using the LSQR-TSVD method. (a3)~(d3) demonstrate the T_1-T_2 spectra inverted by using the LRSR method.

echo data. For LSQR-TSVD method, window average (WA) method is used for data compression to accelerate inversion process (Dunn and LaTorraca, 1999). Each echo train is compressed to 50 points for inversion.

For 2D inversion, the range of T_1 and T_2 relaxation times is set within the interval of [0.1, 10,000] ms and 50 points are logarithmically distributed in each relaxation time dimension. The inversion results of 2D T_1-T_2 relaxation spectra under different SNRs are considered and compared to that inverted by using BRD and LSQR-TSVD methods. The selection of regularization parameters is listed in Table 7. With the decrease of SNR, the ratio of $\lambda_2/\ \lambda_1$ gradually reduced, reflecting that the RMSE increases with the increased noise level. It is very similar with the conclusion from 1D inversion analysis. The T_1-T_2 relaxation spectra obtained with BRD, LSQR-TSVD and LRSR methods are demonstrated in Fig. 7, respectively.

It can be seen that the resolution of the inverted spectra gradually decreases with the decrease of SNR, compared to the forwarding model. For the spectra obtained with BRD method, each spectral peak is gradually integrated with the decrease of SNR, which is difficult to separate. The spectra obtained from LSQR-TSVD method demonstrate the stability at different SNRs, which is benefit from the LSQR method. However, different with 1D simulation cases, inversion results by using LSQR-TSVD method seem to be affected by the introduction of T_1 dimension. For BRD and LSQR-TSVD methods, the morphology of different fluid components is relatively irregular, leading to aliasing regions in 2D spectra at

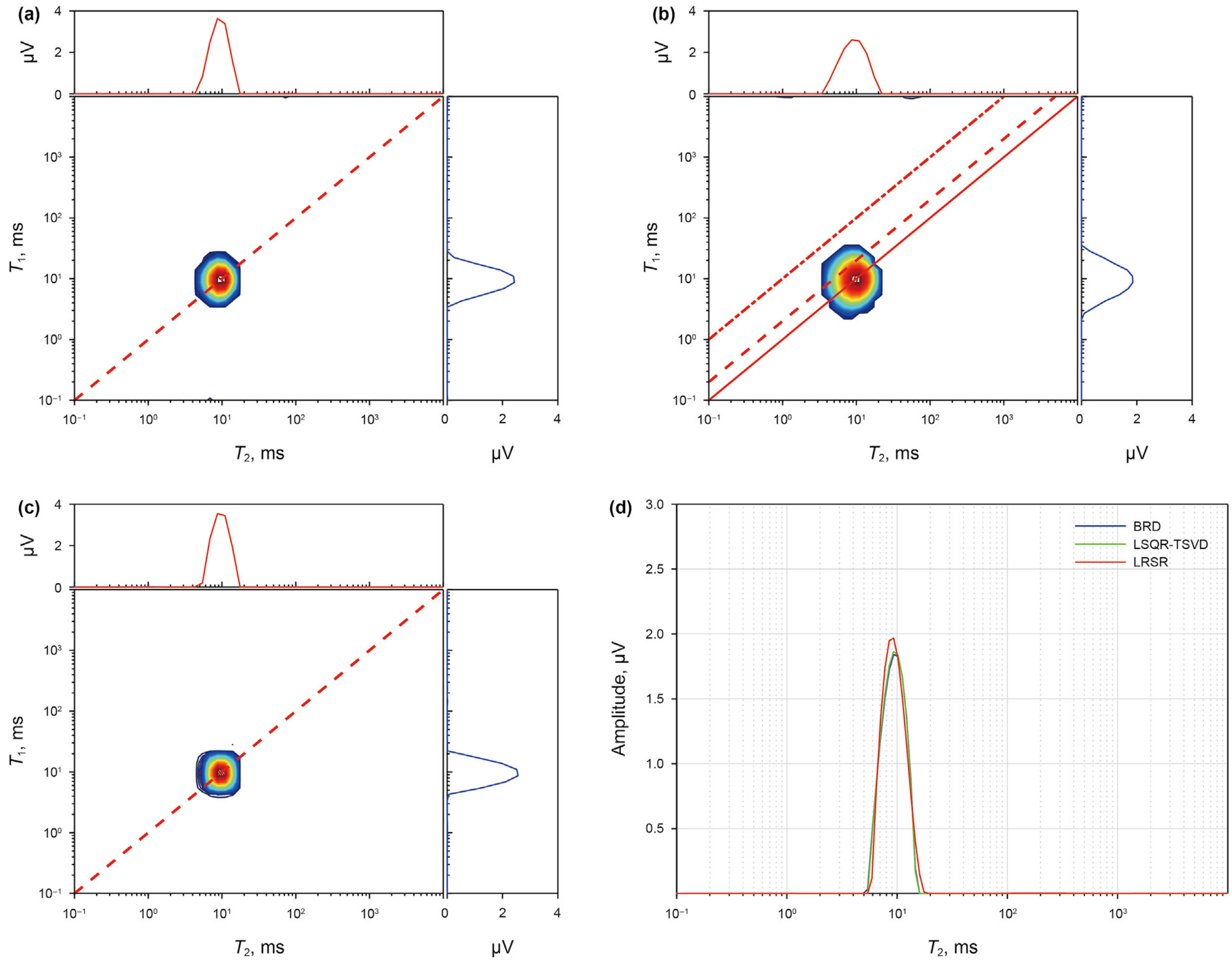

Fig. 8. T_1-T_2 and T_2 spectra of copper sulfate solution obtained by using BRD, LSQR-TSVD and LRSR methods. (a) T_1-T_2 spectra obtained with the BRD method. (b) T_1-T_2 spectra obtained with the LSQR-TSVD method. (c) T_1-T_2 spectra obtained with the LRSR method. (d) T_2 spectrum obtained with BRD, LSQR-TSVD and LRSR methods, respectively.

lower SNRs, even though the peaks in the projection of each T_2 relaxation dimension is identified. For the spectra obtained by LRSR method, the relaxation peaks of different components are symmetrical and highly resolved. It means that the regions of different fluid components can be fully divided, and it is benefit for quantitatively calculating the content of different fluid components. The porosity, RMSE and fluid component content calculated by using BRD, LSQR-TSVD and LRSR methods at different SNRs are listed and demonstrated in Table 6, respectively. The results demonstrate that LRSR method has the advantage to conduct 2D inversion, especially for fluid quantitative identification. The porosity, RMSE and fluid component content are more close to the model. It not only ensures the resolution, but ensures the morphology of the spectra, resulting in improved ability of fluid identification.

4. Experiments and results

Next, the NMR experiments are conducted on free fluids and rock core samples to validate the practical application effects and performance of proposed LRSR method. The tested samples include copper sulfate solution of 10 g, oil-water mixture of 11 g, and artificial sandstone samples. The 1D T_2 and 2D T_1-T_2 experiments are conducted on LIME-MRI-2D 2 MHz Core Analyzer (Beijing Limecho Technology Co., Ltd). The 1D measurements are conducted by using CPMG pulse sequence, and the 2D measurements are conducted by using IR-CPMG pulse sequence. The amplitude of NMR signals and inverted spectra uses microvolt (μV) as unit. In theory, the total area of the spectra is equal to the amplitude of the initial echo measured by NMR instruments.

4.1. Copper sulfate solution

The 1D and 2D inversion results of copper sulfate solution are demonstrated in Fig. 8. For 1D T_2 experiments, the echo spacing is 0.2 ms, echo number is 3000 and signal average is 8 times. For 2D T_1-T_2 experiments, the waiting time is set as 25 steps, which are logarithmically sampled within the interval from 0.1 ms to 5 s. The size of T_1-T_2 spectra is 80*80.

Fig. 8(a)–(c) are the 2D T_1-T_2 inversion results obtained with BRD, LSQR-TSVD and LRSR method, respectively. Fig. 8(d) demonstrates the corresponding T_2 spectra. It can be seen from Fig. 8 that BRD, LSQR-TSVD and LRSR methods have good consistency when free fluid component is measured, and T_2 value of copper sulfate solution is about 10 ms. The SNR is high enough for obtaining high quality spectra with desirable resolution and accuracy. For 2D inversion results, both methods also have good consistency. However, LRSR method demonstrates more symmetrical and regular morphology of spectral peak due to the low-rank and sparsity restraints. On the aspect of calculation precision, the integral area of T_1-T_2 relaxation spectra obtained by BRD method is 12.236 μV and

LSQR-TSVD method is 12.172 μV, while LRSR method is 11.987 μV. Under the condition of sufficient polarization, the signal amplitude measured by NMR instrument is about 11.556 μV. It is validated that the processing result of LRSR is more precise.

4.2. Oil-water mixture

For oil-water mixture, only 2D inversion results are demonstrated and 1D spectra can be reflected by the projections along with T_1 and T_2 dimensions. The 2D inversion results of oil-water mixture are demonstrated in Fig. 9. The acquisition parameters of T_1-T_2 pulse sequence are the same as that used for the measurement of copper sulfate solution, except for the echo number, which is set as 8000 for the sufficient decay of longer relaxation components. Fig. 9(a)–(c) are the inversion results obtained with BRD, LSQR-TSVD and LRSR method, respectively. It is shown that these three methods can better distinguish fluid components with different properties. However, the T_1-T_2 spectra obtained with BRD method reveal a tail along the line of T_1/T_2 of 1 as well as that obtained with LSQR-TSVD method. In addition, the LSQR-TSVD method demonstrates less smoothness. In this case, if the region of fluid component is not separated accurately, it will cause the deviation in the calculation of fluid component content, which is illustrated in the simulation part. In addition, accurate fluid identification needs the sparsity of spectral peaks, which can result in artificial peaks of a few high values due to the noise, and LRSR method may solve this issue. The morphology of spectral peaks is regular and will not produce strong tail morphology, which improves the accuracy of fluid identification. Under the condition of sufficient polarization, the amplitude of T_1-T_2 spectra area obtained with BRD, LSQR-TSVD and LRSR method is 14.133 μV, 14.117 μV and 13.985 μV, respectively. The signal amplitude measured by the instrument is 13.886 μV. It can be seen that the LRSR is more precise for 2D NMR data processing.

4.3. Rock cores

At last, two artificial sandstone samples are tested. The inversion results of two samples are demonstrated in Figs. 10 and 11. Fig. 10(a)–(d) demonstrate the T_1-T_2 and T_2 spectra of sandstone 1, and Fig. 11(a)-(d) demonstrate the T_1-T_2 and T_2 spectra of sandstone 2. These samples have the length of 5 cm and diameter of 2.54 cm and possess different properties. Sample 1 contains chlorite of 10% and its permeability is 100 mD, which is saturated with NaCl solution of 10,000 ppm. The weight porosity of sample 1 is 17.02%. Sample 2 contains illite of 10% and its permeability is 12 mD, which is flooded with #68 oil for one day after the saturation process with NaCl solution of 10,000 ppm. The weight porosity of sample 2 is 22.55%.

In T_1-T_2 experiments, the echo spacing is 0.2 ms, echo number is 4000, and the waiting time is set as 30 steps, which are logarithmically sampled within the interval from 0.1 ms to 3 s. The signal average for sandstone 1 is 16 and for sandstone 2 is 32. In addition, the size of T_1-T_2 spectra is 80*80. The T_2 experiments are also conducted as the comparison group, the size of T_2 spectrum is 80. Echo number is 5000. Echo spacing is 0.2 ms. Waiting time is 3 s. The signal averages for sample 1 is 16 and for sample 2 is 32. In this subsection, only fluid-identification capability of proposed method is discussed.

Fig. 10 demonstrates that there are three fluid components in sandstone sample 1, as three peaks pointed out. Due to the presence of clay mineral like chlorite in sample 1, the left peak (about 2.4 ms) indicates that there exists clay bound water. The middle (about 24 ms) and right peak (about 100 ms) is the capillary bound water and free water, respectively. In the conventional sandstone,

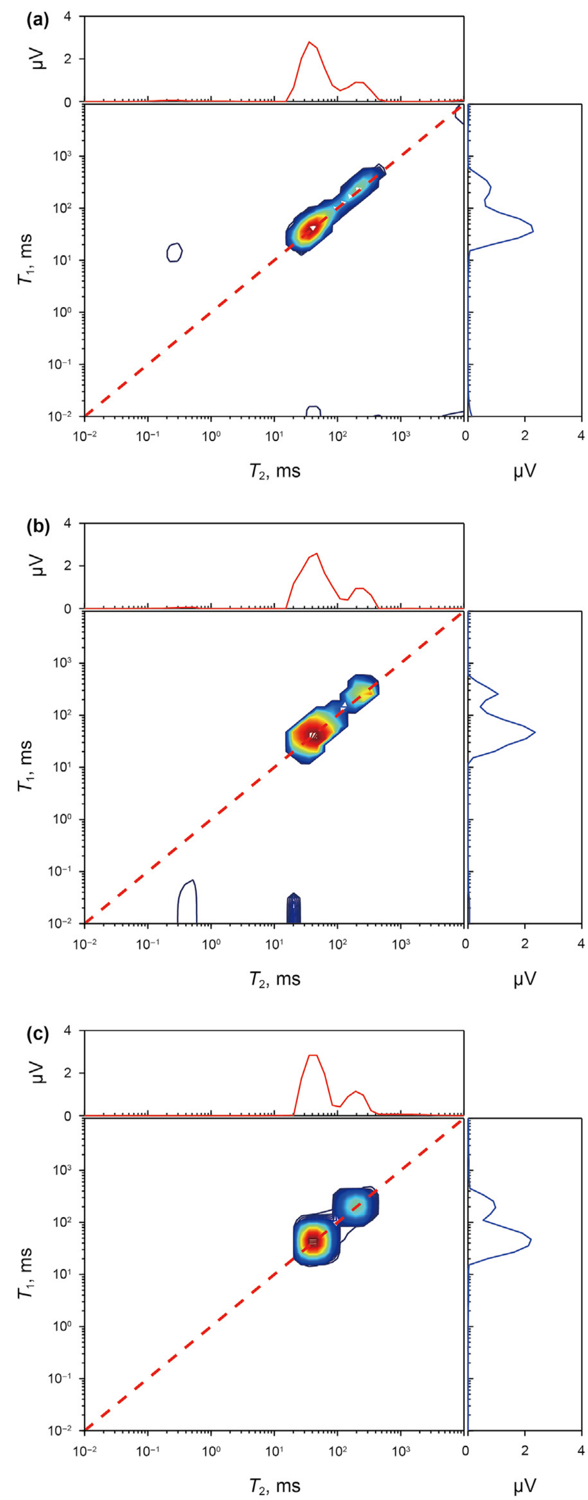

Fig. 9. 2D Inversion results of oil-water mixture. (a) T_1-T_2 spectra obtained with the BRD method. (b) T_1-T_2 spectra obtained with the LSQR-TSVD method. (c) T_1-T_2 spectra obtained with the LRSR method.

an empirical knowledge can be accepted that T_2 value less than 33 ms indicates the capillary bound water, and T_2 value larger than 33 ms indicates the free water (Coates et al., 1999). The T_2 spectrum also validate the accuracy of T_1-T_2 spectra. The projected T_2 spectrum of each T_1-T_2 spectra is in agreement with its corresponding T_2 spectrum. However, due to the limitation of resolution, BRD

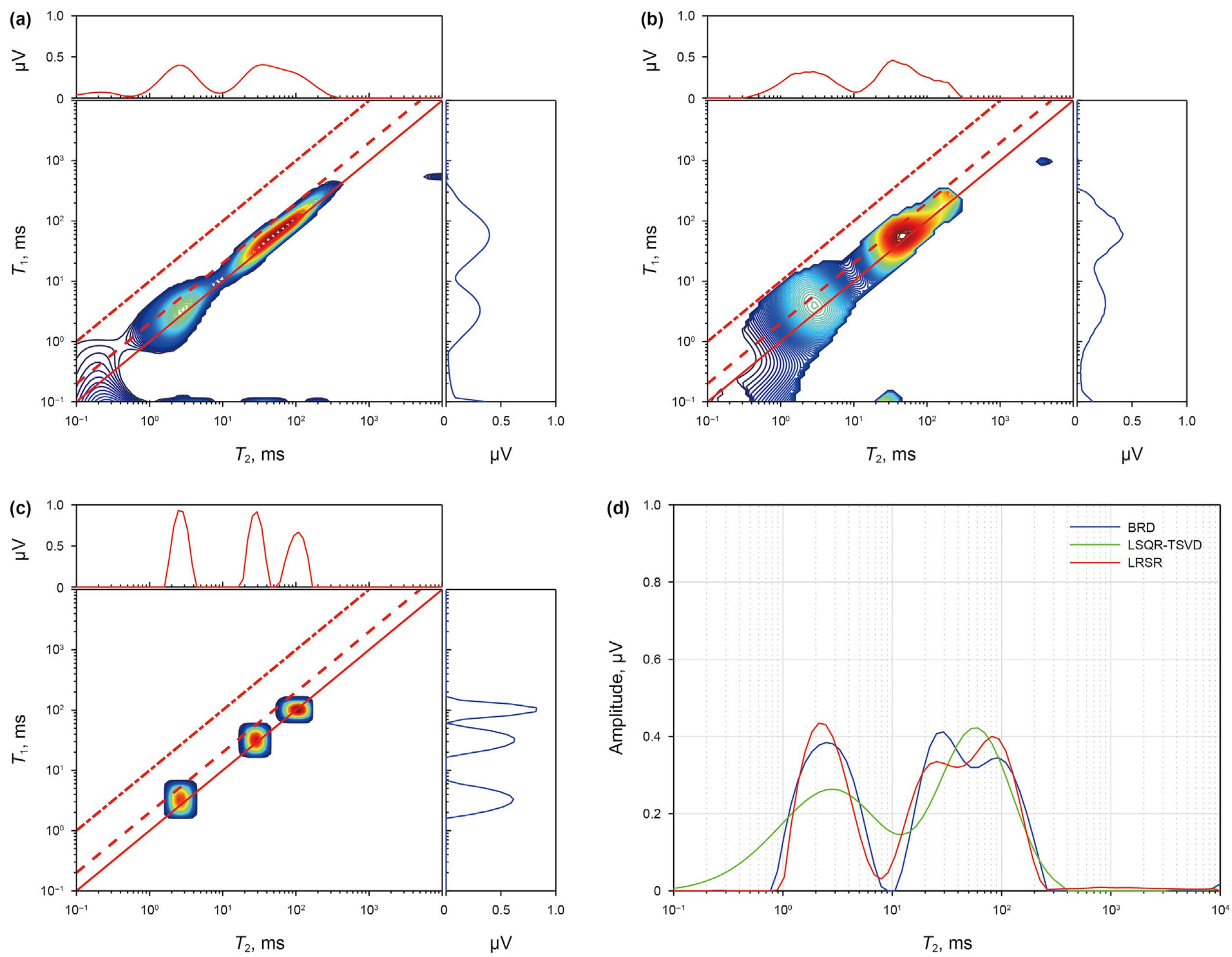

Fig. 10. 2D T_1-T_2 spectra and 1D T_2 spectra of synthetic sandstone sample 1. (a) T_1-T_2 spectra inverted by using the BRD method. (b) T_1-T_2 spectra inverted by using the LSQR-TSVD method. (c) T_1-T_2 spectra inverted by using the LRSR method. (d) T_2 spectrum inverted by using BRD, LSQR-TSVD and LRSR methods, respectively.

(Fig. 10(a)) and LSQR-TSVD (Fig. 10(b)) methods can not clearly distinguish those fluid components with different occurrence state on corresponding T_1-T_2 spectra. Due to the lack of regularization term, T_2 spectrum inverted by LSQR-TSVD method can not separate the capillary water and free water. In addition, artificial peaks are appeared, leading to overestimation of the amplitude, as illustrated in Table 8. It means that the porosity will be overestimated if the signal amplitude has been calibrated into porosity. Fig. 10(c) demonstrates the inversion results obtained with LRSR method. It is clearly observed that the three peaks are highlighted and fluid components are distinguished in vivid. Because the features of 2D T_1-T_2 relaxation spectra are fully extracted with LRSR method, different water components can be determined accurately.

Fig. 11 also demonstrates that there are three fluid components in sandstone sample 2, as three peaks pointed out. In the T_1-T_2 spectra, the T_1/T_2 is around 2, which is not in agreement with the commonly used values for water or oil identification. This may be resulted from the magnetic impurity in this artificial sandstone sample, leading to the relaxation spectra shifted into the short relaxation times. For fluid identification, a first look can be focused on Fig. 11(d). Due to the flooding process, the water in the larger pores is flooded out by #68 oil. The left peak indicates the clay bound water (about 1.6 ms) due to the presence of illite. The middle peak (about 19 ms) and right peak (about 60 ms) in Fig. 11(d) can be clearly distinguished using BRD and LRSR methods except for using LSQR-TSVD method, since LSQR-TSVD method is lack of sparsity. The sandstone is water-wet so that the #68 oil is bulk relaxation time dominated in the large pores, which may result in two peaks for the indication of water and #68 oil. For T_1-T_2 spectra, the BRD method demonstrates the low resolution due to the norm smoothness (as shown in Fig. 11(a)). In contrast, the LRSR method demonstrates good results (as shown in Fig. 11(c)). The LRSR method can improve the resolution of spectra while make spectra much more vivid without artificial peaks disturbed as possible. In addition, the morphology of inverted spectra (relaxation peaks) is very symmetrical and regular, which is benefit for the quantitative fluid-identification and obtaining more precise results. In a summary, the calculated integral amplitude of both T_1-T_2 and T_2 spectra area by using the three methods are compared in Table 8. It can be seen that the LRSR method is more precise for 1D and 2D NMR data processing.

5. Conclusions

The NMR relaxation spectra with high quality and resolution are very important for the qualitative analysis and evaluation of the detected samples. In this paper, a novel method is proposed to effectively improve the resolution and accuracy of 1D and 2D NMR relaxation spectra. The effectiveness and robustness of the proposed method are verified by numerical simulations and practical

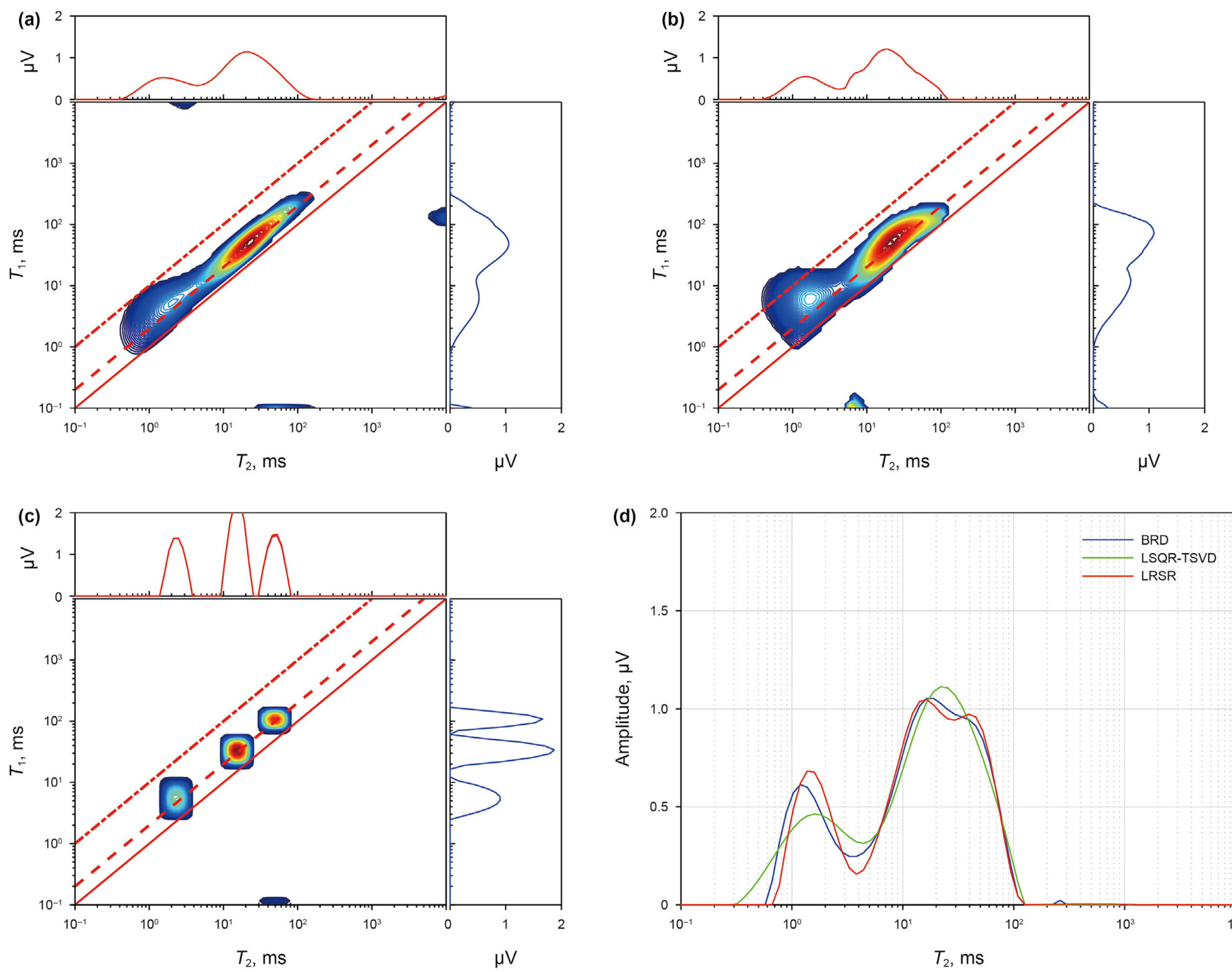

Fig. 11. 2D T_1-T_2 spectra and 1D T_2 spectra of synthetic sandstone sample 2. (a) T_1-T_2 spectra inverted by using the BRD method. (b) T_1-T_2 spectra inverted by using the LSQR-TSVD method. (c) T_1-T_2 spectra inverted by using the LRSR method. (d) T_2 spectrum inverted by using BRD, LSQR-TSVD and LRSR method, respectively.

Table 8
Comparison of the integral amplitude of T_1-T_2 and T_2 spectra area, and the NMR measurement.

Label	BRD, μV	LSQR-TSVD, μV	LRSR, μV	Measurement, μV
T_1-T_2 Inversion				
Sample 1	10.489	10.168	10.139	9.782
Sample 2	22.056	21.671	21.438	20.168
T_2 Inversion				
Sample 1	9.953	9.916	9.874	9.782
Sample 2	21.303	21.271	21.012	20.168

NMR experiments. Here are the conclusions:

(1) The proposed method is based on low-rank and sparsity restraint, which can fully extract the characteristics of the relaxation spectra with low-rank property and improve the resolution with high sparsity. The region of different fluid components can be more clearly separated and distinguished, leading to better application effects of fluid identification and quantification.
(2) The proposed method also has the performance with good noise resistance. The accuracy of spectra can help to improve the precision of physical parameters at low SNRs.

Compared with conventional methods, the LRSR method has the potential to become a general inversion method, which can be applied to NMR relaxation data processing and quantitative analysis. It may play an important role in NMR data processing and interpretation applications, especially in the scenarios like unconventional and complex oil and gas reservoirs. Further NMR petrophysical studies based on the LRSR method will carried on in the future.

Acknowledgements

This paper is supported by “National Natural Science Foundation of China (Grant No. 42204106)”, “China Postdoctoral Science Foundation (Grant No. 2021M700172)”, “The Strategic Cooperation Technology Projects of CNPC and CUP (Grant No. ZLZX2020-03)” and “Natural Science Foundation of the Jiangsu Higher Education Institutions of China (Grant No. 20KJD430002)”. Thanks for Dr. Y.L. Zou and Mr. J.W. Zhang for the discussion of NMR inversion processing.

References

Berman, P., Levi, O., Parmet, Y., et al., 2013. Laplace inversion of low-resolution NMR relaxometry data using sparse representation method. Concepts Magn. Reson. 42 (3), 72–88. https://doi.org/10.1002/cmr.a.21263.
Borgia, G.C., Brown, R.J.S., Fantazzini, P., 2000. Uniform-penalty inversion of

multiexponential decay data: II. Data spacing, T_2 data, systematic data errors, and diagnostics. J. Magn. Reson. 147 (2), 273–285. https://doi.org/10.1006/jmre.2000.2197.

Butler, J.P., Reeds, J.A., Dawson, S.V., 1981. Estimating solutions of first kind integral equations with nonnegative constraints and optimal smoothing. SIAM J. Numer. Anal. 18 (3), 381–397. https://doi.org/10.1137/0718025.

Cai, J.F., Candés, E.J., Shen, Z., 2010. A singular value thresholding algorithm for matrix completion. SIAM J. Optim. (4), 1956–1982. https://doi.org/10.1137/080738970.

Carr, H.Y., Purcell, E.M., 1954. Effects of diffusion on free precession in nuclear magnetic resonance experiments. Phys. Rev. 94 (3), 630–638. https://doi.org/10.1103/physrev.94.630.

Casanova, F., Perlo, J., Blümich, B., 2011. Single-sided NMR. Springer.

Chouzenoux, E., Moussaoui, S., Idier, J., et al., 2010. Efficient maximum entropy reconstruction of nuclear magnetic resonance T_1-T_2 spectra. IEEE Trans. Signal Process. 58 (12), 6040–6051. https://doi.org/10.1109/ICASSP.2010.5495720.

Coates, G.R., Xiao, L.Z., Prammer, M.G., 1999. NMR Logging Principles and Applications. Gulf Professional Publishing.

Du, Q.J., Xiao, L.Z., Zhang, Y., et al., 2020. A novel two-dimensional NMR relaxometry pulse sequence for petrophysical characterization of shale at low field. J. Magn. Reson. 310, 106643. https://doi.org/10.1109/LGRS.2018.2872111.

Dunn, K.J., LaTorraca, G.A., 1999. The inversion of NMR log data sets with different measurement errors. J. Magn. Reson. 140 (1), 163. https://doi.org/10.1006/jmre.1999.1837, 161.

Gao, L., Xie, R.H., Guo, J.F., et al., 2020. A nuclear magnetic resonance echo data filter method based on gray-scale morphology. Geophysics 86 (1). https://doi.org/10.1190/geo2019-0328.1, 1JF–V89.

Ge, X.M., Fan, Y.R., Li, J., et al., 2015. Noise reduction of nuclear magnetic resonance (NMR) transversal data using improved wavelet transform and exponentially weighted moving average (EWMA). J. Magn. Reson. 251, 71–83. https://doi.org/10.1016/j.jmr.2014.11.018.

Ge, X.M., Wang, H., Fan, Y.R., et al., 2016. Joint inversion of T_1-T_2 spectrum combining the iterative truncated singular value decomposition and the parallel particle swarm optimization algorithms. Comput. Phys. Commun. 198, 59–70. https://doi.org/10.1016/j.cpc.2015.09.003.

Gu, M.X., Xie, R.H., Xiao, L.Z., 2021. A novel method for NMR data denoising based on discrete cosine transform and variable length windows. J. Petrol. Sci. Eng. 207, 108852. https://doi.org/10.1016/j.petrol.2021.108852, 2021.

Guo, J.F., Xie, R.H., Xiao, L.Z., et al., 2019. Nuclear magnetic resonance T_1-T_2 inversion with double objective functions. J. Magn. Reson. 308, 106562. https://doi.org/10.1016/j.jmr.2019.07.049.

Guo, J.F., Xie, R.H., Zou, Y.L., 2018. A new method for NMR data inversion based on double-parameter regularization. Geophysics 83 (5), JM39–JM49. https://doi.org/10.1190/geo2017-0394.1.

Hürlimann, M.D., Venkataramanan, L., 2002. Quantitative measurement of two-dimensional distribution functions of diffusion and relaxation in grossly inhomogeneous fields. J. Magn. Reson. 157 (1), 31–42. https://doi.org/10.1006/jmre.2002.2567.

Hursa, G., Silva, Andre, Steene, M.V., Mutina, A., 2020. Learnings from New Slim Hole LWD NMR Technology. International Petroleum Exhibition & Conference. https://doi.org/10.2118/202897-MS. Abu Dhabi, UAE, Nov 9-12.

Jin, G.W., Xie, R.H., Xiao, L.Z., 2020. Nuclear magnetic resonance characterization of petrophysical properties in tight sandstone reservoirs. J. Geophys. Res. Solid Earth 125, e2019JB018716. https://doi.org/10.1029/2019JB018716.

Jin, G.W., Xie, R.H., Xu, H.J., et al., 2019. A new method of NMR echo data inversion constrained by priori information. J. China Univ. Petrol. (Ed. Nat. Sci.) 43 (2), 53–60. https://doi.org/10.3969/j.issn.1673-5005.2019.02.006.

Johns, M.L., Fridjonsson, E.O., Vogt, S.J., Haber, A., 2013. Mobile NMR and MRI: Developments and Applications. Royal Society of Chemistry.

Liang, C., Xiao, L.Z., Zhou, C.C., et al., 2019. Wettability characterization of low-permeability reservoirs using nuclear magnetic resonance: an experimental study. J. Petrol. Sci. Eng. 178, 121–132. https://doi.org/10.1016/j.petrol.2019.03.014.

Lin, Z.C., Chen, M.M., Wu, L., Ma, Y., 2010. The Augmented Lagrange Multiplier Method for Exact Recovery of Corrupted Low-Rank Matrices. https://doi.org/10.1016/j.jsb.2012.10.010. UIUC Technical Report UILU-ENG-09-2215, arxiv: 1009.5055.

Liu, B., Jiang, X.W., Bai, L.H., Lu, R.S., 2021. Investigation of oil and water migrations in lacustrine oil shales using 20 MHz 2D NMR relaxometry techniques. Petrol. Sci. https://doi.org/10.1016/j.petsci.2021.10.011.

Liu, K.Q., Yang, X.S., Zhang, H., et al., 2021. Pore connectivity of oil well cement in the early hydration stage by in situ electrical resistivity measurements and low-field nuclear magnetic resonance. Construct. Build. Mater. 303, 124448. https://doi.org/10.1016/j.conbuildmat.2021.124448.

Lu, C.Y., Feng, J.S., Yan, S.C., Lin, Z.C., 2018. A unified alternating direction method of multipliers by majorization minimization. IEEE Trans. Pattern Anal. Mach. Intell. 40, 527–541. https://doi.org/10.1109/TPAMI.2017.2689021.

Luo, S.H., Xiao, L.Z., Jin, Y., et al., 2022. A machine learning framework for low-field NMR data processing. Petrol. Sci. https://doi.org/10.1016/j.petsci.2022.02.001.

Meiboom, S., Gill, D., 1958. Modified spin-echo method for measuring nuclear relaxation times. Rev. Sci. Instrum. 29 (8), 688. https://doi.org/10.1063/1.1716296.

Mitchell, J., Chandrasekera, T.C., Gladden, L.F., 2012. Numerical estimation of relaxation and diffusion distribution. Prog. Nucl. Mag. Res. Sp. 62, 34–50. https://doi.org/10.1016/j.pnmrs.2011.07.002.

Pang, X.J., Wang, G.W., Kuang, L.C., et al., 2017. Insights into the pore structure and oil mobility in fine-grained sedimentary rocks: the Lucaogou Formation in Jimusar Sag, Junggar Basin, China. Mar. Petrol. Geol. 137, 105492. https://doi.org/10.1016/j.marpetgeo.2021.105492.

Parasram, T., Daoud, Rebecca, Xiao, D., 2021. T_2 analysis using artificial neural networks. J. Magn. Reson. 325, 106930. https://doi.org/10.1016/j.jmr.2021.106930.

Prammer, M.G., 1994. NMR pore size distributions and permeability at the well site. In: SPE Annual Technical Conference and Exhibition. Louisiana, New Orleans. https://doi.org/10.2118/28368-MS. Sepp. 25–28.

Prange, M., Song, Y.Q., 2009. Quantifying uncertainty in NMR T_2 spectra using Monte Carlo inversion. J. Magn. Reson. 196, 54–60. https://doi.org/10.1016/j.jmr.2008.10.008.

Qu, X.B., Mayzel, M., Cai, J.F., et al., 2015. Accelerated NMR spectroscopy with low-rank reconstruction. Angew. Chem. Int. Ed. 54 (3), 852–854. https://doi.org/10.1002/anie.201409291.

Reci, A., Sederman, A.J., Gladden, L.F., 2017. Obtaining sparse distribution in 2D inverse problems. J. Magn. Reson. 281, 188–198. https://doi.org/10.1016/j.jmr.2017.05.010.

Siavashi, J., Najafi, A., Sharifi, M., et al., 2022. An insight into core flooding experiment via NMR imaging and numerical simulation. Fuel 318, 123589. https://doi.org/10.1016/j.fuel.2022.123589.

Singer, P.M., Asthagiri, D., Chapman, G., Hirasaki, G.J., 2017. Molecular dynamics simulations of NMR relaxation and diffusion of bulk hydrocarbons and water. J. Magn. Reson. 277, 15–24. https://doi.org/10.1016/j.jmr.2017.02.001.

Song, Y.Q., Kausik, R., 2019. NMR application in unconventional shale reservoirs—a new porous media research frontier. Prog. Nucl. Magn. Reson. Spectrosc. 112–113, 17–33. https://doi.org/10.1016/j.pnmrs.2019.03.002.

Song, Y.Q., Venkataramanan, L., Hürlimann, M.D., et al., 2002. T_1-T_2 correlation spectra obtained using a fast two-dimensional Laplace inversion. J. Magn. Reson. 154 (2), 261–268. https://doi.org/10.1006/jmre.2001.2474.

Su, G.Q., Zhou, X.L., Wang, L.J., et al., 2016. An inversion method of 2D NMR relaxation spectra in low fields based on LSQR and L-curve. J. Magn. Reson. 265, 146–152. https://doi.org/10.1016/j.jmr.2016.01.024.

Tan, M.J., Zou, Y.L., Zhang, J.Y., et al., 2012. Numerical simulation of (T_2, T_1) 2D NMR and fluid responses. Appl. Geophys. 9 (4), 401–413. https://doi.org/10.1007/s11770-012-0351-3.

Wang, P., Venkataramanan, L., Jain, V., 2017. Sparse clustered Bayesian-inspired T_1-T_2 inversion from borehole NMR measurements. IEEE Transact. Comput. Imag. 3 (3), 355–368. https://doi.org/10.1109/TCI.2017.2693562.

Xiao, L.Z., Liu, H.B., Deng, F., et al., 2013. Probing internal gradients dependence in sandstones with multi-dimensional NMR. Microporous Mesoporous Mater. 178, 90–93. https://doi.org/10.1016/j.micromeso.2013.04.003.

Xie, R.H., Xiao, L.Z., 2011. Advanced fluid-typing methods for NMR logging. Petrol. Sci. 8, 163–169. https://doi.org/10.1007/s12182-011-0130-4.

Xie, R.H., Wu, Y.B., Liu, K., et al., 2015. Using wavelet-domain adaptive filtering to improve signal-to-noise ratio of nuclear magnetic resonance log data from tight gas sands. Geophys. Prospect. 64 (3), 689–699. https://doi.org/10.1111/1365-2478.12333.

Zhao, P., He, B., Zhang, B., Liu, J., 2021. Porosity of gas shale: is the NMR-based measurement reliable? Petrol. Sci. https://doi.org/10.1016/j.petsci.2021.12.013.

Zhou, X.L., Su, G.Q., Wang, L.J., et al., 2017. The inversion of 2D NMR relaxometry data using l_1 regularization. J. Magn. Reson. 275, 46–54. https://doi.org/10.1016/j.jmr.2016.12.003.

Zhuang, L.S., Gao, H.Y., Lin, Z.C., et al., 2012. Non-negative low rank and sparse graph for semi-supervised learning. IEEE Conf. Comp. Vision and Patt. Recognit. https://doi.org/10.1109/CVPR.2012.6247944.

Zou, Y.L., Xie, R.H., Ding, Y.J., et al., 2015. Inversion of nuclear magnetic resonance echo data based on maximum entropy. Geophysics 81 (1), D1–D8. https://doi.org/10.1190/geo2015-0200.1.

Zou, Y.L., Xie, R.H., Liu, M., et al., 2018. Nuclear magnetic resonance spectrum inversion based on the residual hybrid l_1/l_2 norm. Geosci. Rem. Sens. Lett. IEEE 15 (8), 1194–1198. https://doi.org/10.1109/LGRS.2018.2835457.